NASA Contractor Report 198352

A Study of Facilities and Fixtures for Testing of a High Speed Civil Transport Wing Component

J. A. Cerro, R. F. Vause, L. M. Bowman, J. K. Jensen, C. J. Martin, Jr., A. E. Stockwell and W. A. Waters, Jr.
Lockheed Martin Engineering and Science Services, Hampton, Virginia

NAS1-19000

July 1996

National Aeronautics and
Space Administration
Langley Research Center
Hampton, Virginia 23681-0001

CONTENTS

INTRODUCTION

The High Speed Research (HSR) Component Structures element has a goal to test a large-scale wing component in fiscal year 2001. Figure 1 shows the location of the main wing box section in the McDonnell Douglas High Speed Civil Transport (HSCT), and figure 2 shows the proposed wing box component test article. In order to prepare for this test, a study was performed to determine the existing capabilities in the Structures and Materials Testing Laboratory in Building 1148 at the NASA Langley Research Center. The report includes a survey of the electrical and hydraulic resources in Building 1148 and identifies the backing structure and floor hard points which would be available for reacting the test loads. The backing structure analysis includes a new finite element model of the floor and backstop support system in the Structures Laboratory. Information on the data acquisition system and the thermal power requirements is also presented.

The study identified the hardware that would be required to test a typical component, including the number and arrangement of hydraulic actuators required to simulate expected flight loads. Load introduction and reaction structure concepts were analyzed to investigate the effects of experimentally induced boundary conditions.

The information in this document was compiled with the help of many people at LaRC, both civil servants and contractors. To all who have helped, the authors express their appreciation.

SECTION I

FACILITY SURVEY

Data Acquisition System

The future data acquisition capabilities for the Structural Mechanics and Thermal Structures Branches will include five systems. The Combined Loads Test System (COLTS) will have three 512-channel systems. The Structures and Materials Testing Laboratory in Building 1148 will have two systems. One of these systems, the MODCOMP system, is currently in use for large-scale structural tests and has a 300-channel capability. Future plans involve the addition of another 350-channel system. Each system in Building 1148 will be upgraded to 512-channels with one system being used for reading strain gages and the other for reading thermocouples. There will be a patching capability for using multiple data acquisition systems simultaneously.

The data sampling rate for the acquisition systems will probably exceed requirements. Thus the system limitation would be driven more by how much memory is available for storing the data. Typically for static loading, the data is sampled at one frame per second. The data is initially stored on the MODCOMP system and later transferred to one of the branch's UNIX-based computer systems. Future plans indicate that test data will ultimately be stored on a large capacity disk & jukebox system.

Signal conditioners are now used in the current data acquisition systems, replacing the older balance/calibration racks. This will be the system used for the HSR wing box test. The analog-to-digital converters will be similar to those used on the older Beckman data acquisition system.

Instrumentation Issues

Selections of strain gages and thermocouples will be determined on the basis of expected temperature and strain conditions. These should be determined as early as possible as there may be a lead time problem in ordering these from the vendor.

Expected displacement fields need to be determined to aid in the selection of displacement transducers or Direct-Current Differential Transformers (DCDT's). DCDT's currently in use for similar tests fall into two categories: 1-inch stroke, and 22-inch. stroke. A sufficient quantity of the 1-inch stroke probes will probably be available for the purposes of testing the wing box specimen. The existing 22-inch stroke displacement probes are manufactured by Schlumberger. Fifteen of these are located in Building 1148, and approximately twenty more are located at the Building 1160 test facility (Pressure Box). These probes are designated for use at the COLTS Facility when it is brought on line. It is necessary to determine the ordering requirements for these probes if the existing quantity is insufficient due to a projected two year lead time in ordering them from the vendor.

For elevated temperature tests, the barrels of the displacement probes should be located outside the heated areas. The moveable cores should be attached to a rod which attaches to the heated surface of the specimen. The rods should be made of glass, quartz, or graphite to withstand the high temperatures.

Hydraulic Jack/Actuator System

Preparations are being made to test a composite semi-span wing in 1998. This specimen will use as many as eight loading jacks/actuators. Details concerning control of the jack/actuator array are still to be determined. There are several options available. It is possible to have a primary actuator determine the loading of the other actuators in the loop. Another possibility is to have the entire jack/actuator array controlled using a general-purpose software package such as LabVIEW. The technique employed in the mechanical loading of this wing semi-span will be directly applicable to the HSR wing box.

The loading scheme for the HSR wing box specimen will need to be determined in order to select the jacks/actuators used during the test. The necessary stroke dimension is also a critical parameter. Telescoping-type actuators should be considered for long stroke lengths. A wing stub box was recently tested in Building 1148 using a 300,000-lb capacity non-telescoping type hydraulic actuator with a 24-inch stroke manufactured by Shore Western. Figure 3 shows the dimensions of the actuator assembly. The entire height of this jacking arrangement, including the thickness of the specimen was approximately 14 feet. The top of the slotted plate on the Building 1148 backstop is currently 15 ft. This assembly nearly represents the practical limit of the current building/backstop configuration for the non-telescoping type actuator. Longer stroke requirements will probably necessitate a telescoping-type actuator configuration.

Selections of pumps and vendors of various components can be determined after a loading method is selected. The following equipment may be available from COLTS: four 125,000-lb actuators with a 12-inch stroke, and four 125,000-lb actuators with a 24-inch stroke. Additionally, there may be four 225,000-lb actuators with a 12-inch stroke available for use. These actuators would come from the pressure box facility.

The load cells employed should be matched to their respective jacks and actuators. The previous test of the composite wing stub box from McDonnell Douglas utilized a 300,000-lb load cell matched to the 300,000-lb Shore-Western actuator.

The entire jacking mechanism consisting of the actuators, swivels, load cells, and attachment blocks should be located inside a cage-type framework. This safety feature is needed to prevent the assembly from toppling during specimen failure. It was employed in Building 1148 during the recent test of the McDonnell Douglas Wing Stub Box. This assembly is shown at the Figure 4. The square-tube framework shown in this figure was necessary for mounting

DCDT's and other instrumentation and to suspend a safety harness strap under the wing to prevent it from falling to the floor during failure.

Electrical System

The present electrical power in Building 1148 is 440 volts, 3 phase at 200 amps. There are two substations currently serving this building. The 2000 KVA substation has 1600 KVA (1.6 MW) available at 480 VAC. Recent energy consumption plots show a maximum of 400 KVA used for a typical day. The 200 KVA substation has 200 KVA (0.2 MW) available at 480 VAC. Plots indicate a maximum consumption of 300 KVA for a typical day.

The Building 1148 electrician recommends that the 200 KVA substation not be relied upon as a source of power. The electrician also suggests we have 0.5 MW and may have as much as 1 MW of electrical power available. A discussion with the Building 1148 technician indicated that there is no emergency back-up electrical power in the building sufficient for running a series of experiments of this magnitude.

Heating System

Although the heating system design was not part of this task, a brief survey of heating system power requirements is presented in this section. Two heating systems were reviewed—quartz lamp arrays and heater blankets.

The quartz lamp arrays provide a radiant heat source and achieve temperatures up to 4000° F. Quartz lamps require reflector shields and proper spacing to achieve the appropriate temperature distributions and also create large power losses due to conduction, convection, and radiation. Several thermal structural tests have been conducted in the past several years at NASA Dryden laboratory where quartz lamp arrays have been used. For example, 496 quartz lamps with a 12 inch length were used to heat a 52 square foot X-15 horizontal stabilizer to temperatures in the 3000° F range (ref 4). In comparison, the proposed HSCT wing box test specimen has a minimum area of 600 square feet and would require at least 1000 quartz lamps with a 24 inch length to reach temperatures in the 300° F range.

Heater blankets provide a conduction heat source and achieve temperatures up to 1200° F. Heater blankets are a combination of heater and fiberglass insulation layers. They can be attached to a structure by use of mechanical fasteners. In contrast to quartz lamps, the heater blanket power losses are primarily due to convection and are relatively small. The heater blankets are available in standard and custom sizes. The HSCT wing box test would require at least 72 blankets that are 2 feet by 4 feet. The calculations in Appendix A show that 0.25 MW would be consumed by the heater blankets at the test temperature of 350° F. This is within the current B1148 electrical capacity.

An additional concern was that the backstop would act as a large heat sink, resulting in increased power requirements for maintaining the wing at the test temperature. A temperature increase in the mild steel backstop could also reduce material properties. An estimate of the heat loss to the backstop, contained in Appendix A, indicates that with a 12 inch mild steel connecting section, heat losses through conduction to the backstop are only 4 kW. This is insignificant compared to the total heating power requirements and should not produce much of a temperature rise in the massive backstop structure. Heating losses could be further minimized by using insulating spacers.

Backstop/Floor Support System

The backstop/floor support structure in the Building 1148 Structures Lab is basically a cantilever support structure. This structure must safely resist loads applied by a test article (particularly bending moment) and deform very little under these loads. The basic components of the structure are shown in figure 5. Information on the structure was obtained from

fabrication drawings, foundation drawings, and field measurements. Reference drawings were obtained from the NASA Langley Facilities Engineering. The steel fabrication drawings were produced by the Pittsburgh-Des Moines Steel Company in 1939. The structural details for the columns, floor beams, and mounting plates can be found on drawings SL-1, SL-2, SL-3, and SL-4. Foundation details are illustrated on NASA drawings D8307 and D8327. The overall dimensions of the backstop structure are shown in figure 6. This sketch summarizes much of the information found in the drawings. Detailed information on the column sections, mounting plates and floor beams is depicted in figures 6, 7 and 8 respectively.

The support structure was analyzed to determine if the components could safely resist loads applied by the test article. The stiffness of the support structure was evaluated to determine how well the backstop approximates a 'fixed' test boundary condition, where the support structure does not rotate or translate under applied test loads. The structural model for the backstop structure is shown in figure 9. The entire structure was modeled to allow for general, non-symmetric loads, including all the load cases for the wing-box structure. Figures 10 and 11 show details of the finite element representation of the wing box test article. The wing box model was a simplified version of the model described in Section II of this report. The structure was simplified to reduce the model complexity while providing a reasonable approximation of the overall stiffness. The webs of the columns and floor beams were modeled with shell elements while the flanges were represented with beam elements. The mounting plates were attached to the columns with compatibility links to simulate the bolted connection. A steel plate connected the top of all the backstop columns. Shear webs between the floor beams were used to tie the separate beams together. The shear webs were chosen as a conservative method to spread the load in the y direction since there is top and bottom reinforcing steel running perpendicular to the floor beams. Reactions for the structure are provided at each pile location.

For the backstop/floor analysis, the weight of the structure was included in all applied load cases. Structural weight was important, because the piles were assumed to have zero tensile resistance. A summary of dead weight calculations is presented in Appendix B. Translational restraint was specified in all three directions at each pile location. The piles were assumed to have a 40 kip compressive capacity and zero tensile resistance. A pile spacing of five feet by seven feet was used in the model. This differed slightly from the assumptions made in references 5 and 6. Steel allowable stresses were based on the specifications of reference 1. Concrete shear limits were based on equations from reference 2 and specifications from the American Concrete Institute (ACI). The test load forces were based on the reaction forces calculated in the finite element analysis of the wing box component model (Appendix C).

Results

Several critical areas were checked for excessive loads. Pile loads were checked for allowable compressive stress and for possible tensile stress. Although the piles cannot resist tensile loads, an uplift load on a floor beam would be spread out by the shear webs to adjacent floor beams. Other areas of concern included the backstop column flange stresses, mounting plate bolt loads, mounting plate attachment stresses and floor beam flange stresses.

A 172 kip load (see figure 13) was applied at the tip of the model to simulate the mechanical forces resulting from load case 7, a Mach .95 subsonic pull-up. The vertical deflection at the load point was approximately 32 inches. The lateral deflection at the column tops is shown in figure 14. Maximum lateral deflection is about 0.2 inches at the center top of the backstop. The maximum forces in the front flange of the middle column are shown in Figure 15. These forces can be divided by the 30 square inch area of the flange to obtain stress in ksi. The front flange of the column has the maximum tensile loads since the uplift load combines with the tensile couple force of the overturning moment. The relatively low stresses are consistent with the fact that the backstop was designed to resist larger fuselage bending moments. The pile loads along the middle floor beam are shown in figure 16. All pile loads are

within the estimated twenty ton capacity. The pile loads are smaller on the front side of the column due to the overturning moment generated by the uplift load at the wing tip.

Several of the proposed load cases for the HSR wing box tests would require an uplift load to be applied to the floor beams. The floor beam was evaluated for thread shear-out and bending of the column flanges due to concentrated loads (see figure 8). The maximum allowable uplift load consisted of two 7.5-kip loads being applied to a hole on each side of the beam flange, resulting in a total load of 15 kips. Concentrated load points should be spaced no closer than 36 inches along the beam centerline. The load limiting failure mode was bending of the beam flanges. Testing of a floor uplift location is recommended to provide essential information on strength and stiffness. A sketch of a floor uplift load test rig is shown in figure 12. The sketch is based on an apparatus that was used to test backstop flange loads on a large component test.

Advantage should be taken of several upcoming component tests to gather more data which can be used to monitor the support structure response. For example, a McDonnell Douglas semi-span wing box is scheduled to be tested on the 1148 backstop in fiscal year 1997. A small number of strain gages and displacement transducers could be set up to record the backstop response. These measurements could be correlated with analysis to better define the stiffness properties of the floor beams, concrete, and piles. Uplift loads will be applied to the floor structure during a small wing component test in fiscal year 1996. Strain and displacement measurements in the vicinity of the load could provide useful information for future tests.

SECTION II

TEST SIMULATION

Model Description

A McDonnell Douglas Aircraft Company (MDAC) finite element model (FEM) of a typical HSCT wing box test specimen was delivered to NASA in MSC/NASTRAN format. MSC/PATRAN was used to read in the NASTRAN data files and postprocess the results. Figure 17 is a plot of the MDAC model. For clarity and postprocessing purposes the model was broken into several groups. Figure 18 shows the group created for upper surface plate elements, figure 19 shows a similar group for the lower surface, figure 20 shows all of the internal structure web elements and figure 21 is a plot of all of the one dimensional elements in the model. The latest design variable values supplied with the FEM were used for physical properties. Table 1 summarizes the entities which make up the model. The loads and boundary conditions for twelve flight load conditions were also included with the model data files. A summary description of these twelve load conditions is given in table 2.

Actuator Force Requirements

A goal of this study was to determine the magnitudes and locations of actuator forces necessary to simulate the flight load applied forces. In order to accomplish this, the model was analyzed for all twelve flight condition load cases, and recovered forces and moments were summed for each case using a PATRAN Command Language (PCL) program.

It was assumed that there would be no more than six regions on the test structure where loads would be applied by hydraulic jacks. Based on the wing box geometry, the five regions shown in figure 22 were chosen. They are the tip rib, leading edge, inboard trailing edge, engine pylon and outboard trailing edge. A sixth region, the root rib, was the reaction location for all of the applied mechanical forces. In order to implement the laboratory tests, a backstop-to-specimen interface fixture would be required at the root rib location. This fixture would increase the distance from the tip load application point to the backstop. The wing box internal structure is not shown in figure 22. There were significant flight loads applied to the internal structural

elements, and another group, referred to as "internal structure," was created to tabulate the forces on these elements.

Note that in figure 22 each component has an associated coordinate frame. These coordinate frames were used as the reference frame for summations of forces and moments on their respective components. The moments for each component were summed about the origin of the component's coordinate frame. For example, forces at the tip rib are summed in coordinate system 5. Summing forces for the tip rib resulted in large forces in the Z direction and large moments about the X and Y axes. For the tip rib component a positive Z force represents lift load, and a positive X moment represents wing bending with the upper surface in compression. A negative Y moment represents wing torsion with the leading edge moving in the positive Z direction and the trailing edge moving in the negative Z direction. For each loading condition, table 3 shows a summary of the dominant forces and moments applied to the tip rib, leading edge, engine pylon and internal structure. A complete listing of force summations is given in Appendix C. Forces on the inboard trailing edge and outboard trailing edge components were not included in the tables, because they were small compared to the resultant forces on the other components.

Loading Fixture Arrangements

The mechanical loading requirements summarized in table 3 were used to determine which loading conditions would be suitable for simulation. Hydraulic actuator load and stroke requirements were then determined for each load case. The possibility of eliminating loads at the leading edge, engine pylon and internal structural members was also investigated.

Inspection of internal structural member loads listed in table 3 shows that for three loading conditions, the 9G crash condition and the +/- 8G Gust conditions, large forces were required in the plane of the wing (x and y directions) as well as in the transverse (z) direction. Since these forces consist mostly of uniformly distributed inertial forces, a complex whiffletree type arrangement would be required, and forces would have to be applied in the plane of the wing as well as in the transverse direction. Therefore these three conditions were eliminated from testing consideration. Similarly the seize limit load case, which consists mainly of concentrated loads in the vicinity of engine mounting points, was also eliminated. Eliminating the four non-typical flight load conditions left eight possible load cases--four subsonic maneuvers and four supersonic maneuvers. These conditions are numbered 5 through 12 in table 3.

Using the forces and moments from table 3, a single-point location for applying resultant loads can be calculated for each component to satisfy the shear force, bending moment, and twisting moment requirements of a given load case. For example, to simulate a Mach .95 3.75G subsonic pull-up (load case 7), a shear force of 172,000 pounds, a bending moment of 13.5 million inch-pounds and a twisting moment of -8.39 million inch pounds would have to be applied to the tip rib. This can be achieved by applying a force of 172,000 pounds at a location of (49 79 0) in coordinate frame 5. Actuator locations are given in table 4 for the tip rib and leading edge components. Actuator locations for the engine pylons, and the trailing edge loads were not included in table 4, because these loads were not significant compared to loads on the other components.

Table 4 shows that the leading edge load point location varies only 6.5 inches in x and 8.5 inches in y for the eight load cases. Based on these results, it was assumed that a loading fixture for the leading edge could be designed with a large enough region of travel to allow positioning of a single actuator at the required point for each loading condition. The pylon load has no appreciable applied moments. Therefore only a relatively small interface fixture would have to be designed to input pylon loads at the end of the pylon structure. Although the tip load location varies only 17.5 inches in x and 10.5 inches in y, as shown in table 4, consideration was given to multiple actuator arrangements in order to reduce the large stroke required for a single

actuator. The trade off of the simplicity of a single tip actuator vs. the versatility of a multiple-actuator arrangement was investigated.

Actuator arrangement 1 is shown in figure 23. A single actuator is used at the tip, and a total of only three actuators are required to simulate the mechanical loads applied to the wing box. Force vectors are shown as positive in the lift (z) direction, however some of the applied forces may be negative. For example the engine pylon loading is negative for all of the pull-up maneuvers and positive for all of the pushdown maneuvers. If inertial forces were required over the entire wing box planform, a load distribution mechanism such as a whiffletree would be required. The effect of eliminating the inertial force loads is discussed later in this section. The actuator which supplied force at the tip rib in figure 23 was required to be repositionable to cover the range of locations required for multiple flight conditions. It should be feasible to construct a loading fixture which would handle all eight of the chosen load cases. The tip load application region is indicated (not to scale) by the shaded portion of the tip load-to-wing box transition structure in figure 23. The benefits of actuator arrangement 1 are derived from its simplicity. The single tip load actuator does not require a sophisticated control system to coordinate the operation of multiple hydraulic jacks. In fact if leading edge, pylon, and inertial forces were not critical to the general load distributions in the test specimen, it would be possible to run the 8 test conditions with only the single tip load actuator. However, the relatively large stroke required by this arrangement could exceed the available capabilities. The stroke limit of actuators in use at the Building 1148 structures lab at the time of this study was 24 inches.

To alleviate some of the restrictions of actuator arrangement 1, another arrangement was defined which uses multiple actuators to load the tip rib. Actuator arrangement 2 is depicted in figure 24. Note that this system uses the same actuators as arrangement 1 for the leading edge and pylon loads. For the tip load, two actuators (indicated as forces F1 and F2 in figure 24) are used at a point 45 inches outboard of the tip rib. These actuators are located inboard of the tip actuator location used in arrangement 1 in order to reduce tip displacement and hence the required tip actuator stroke. The two actuators supply shear load and bending moments. Since these two actuators were located inboard of the single-actuator location used in arrangement 1, the total load they applied had to be greater than the load applied by the single tip actuator in order to maintain the required bending moment in the specimen. To maintain the correct shear load in the specimen two more actuators (indicated as forces F3 and F4 in figure 24) were used at the same spanwise station as the tip rib to take out the extra shear load that was supplied by actuators 1 and 2. Actuators 3 and 4 were also used to apply torsional load to the wing box. Actuator arrangement 2 offers the advantage of a more general loading capability which does not require repositioning of actuators. However, a complication exists in the need for a more sophisticated control system to coordinate loading of the 4 actuators at the tip rib. A total of 6 actuators must be controlled, if leading edge and pylon loads are included in a test. Also, actuators 3 and/or 4 would exert uplift loads on the floor for some load cases. The capability of supporting uplift floor loads is addressed in a separate section of this report.

Finite Element Model Modifications

Finite element analyses were performed to determine the difference in internal load distributions for the wing box structure loaded by the flight loads and the laboratory test loads. Two variations of the basic finite element model were required to conduct these analyses.

Figure 25 shows the finite element model for actuator arrangement 1. There is an extension of plate elements to 45 inches outboard of the tip rib. This relatively rigid structure was used to uniformly distribute load from the point of actuator force input into the tip rib structure. For modeling convenience, outboard of 45 inches rigid bar elements are used to connect the tip extension to a single node located at the required point of load application listed in table 2. For purposes of simplicity and rigidity, 0.5 inch thick steel plates were used for all plate elements in this fixture. AISI 4130 steel was used for this structure, because it is a common material for load fixtures and has a thermal expansion coefficient which closely matches the

coefficient for the titanium wing. A different wing specimen material, for example a graphite/epoxy composite system, would probably require a change in material and/or design of the load introduction structure. No additional structure was modeled for the leading edge force input. Only two rigid bars emanating from the point of crank in the leading edge to the point of load application were used in the model. The application point was chosen to allow the applied load to be carried by the only interior rib that intersects the leading edge. Loading the leading edge at a rib location will help to better distribute forces into the wing box. Only a small fixture would have to be designed to clamp onto the leading edge at this location. The fixture would extend to the point of load application as defined in table 2 and be large enough to accommodate the 6.5 inch to 8.5 inch variation in location of actuator force. Engine pylon loads were applied through a small fixture centering the load at the rear of the engine pylon.

Modeling of actuator arrangement 2 is shown in figure 26. This model was the same as the model shown in figure 25, except that the rigid bars connecting the tip extension to the point of load application were removed. The tip actuator load was applied by forces F1 and F2, and the excess shear was removed by forces F3 and F4 applied at the tip rib. Actuators 3 and 4 were also used to supply a wing torsional moment.

Point forces and moments which were supplied as flight loads for the Mach .95 3.75G pull-up maneuver are shown in figures 27, 28, and 29 to illustrate a typical load distribution. This load condition was dominated by spanwise wing bending, as indicated by the large load vectors along the top and bottom edges of the root and tip ribs. Both actuator arrangements would adequately simulate this bending behavior. Other significant forces were inertial forces along the leading edge and at the engine pylon. The applied concentrated moments shown in figure 28 were not simulated by either actuator arrangement 1 or 2. Figure 29 shows why some type of whiffletree arrangement would be required to simulate the inertial loading on the wing box's internal structural members.

Analysis Results

The first load case to be analyzed for internal load distribution was the Mach .95 3.75G subsonic pull-up condition. This is a 2.5G limit load condition multiplied by a safety factor of 1.5. Figure 30 shows the distribution of internal element forces in terms of spanwise running load in the upper surface panels, torsional shear load in the upper surface panels, shear load in the spar webs and Z displacement (through-thickness direction) plotted on the upper surface panels. These four plots were used to judge the acceptability of applying loads with actuators to simulate the analytically predicted flight loads. Results presented in figure 30 are for the Mach .95 3.75G pull-up condition using the flight loads, but restraining the root rib as though it were rigidly connected to the backstop. This was considered the baseline condition for this particular load case and actuator loadings were designed to try to match the load distributions presented in figure 30.

Figure 31 presents the results of a simulation of the Mach .95 3.75G pull-up condition using the actuator arrangement of figure 23. The tip rib actuator applied a 171,600 pound load, the leading edge actuator applied a 42,300 pound load, and the engine pylon actuator pulled down with 27,800 pounds of force. The inertial loads (see figure 29) were included in this analysis so that comparisons could be made with the results shown in figure 30 for the flight loads. The effect of removing these inertial loads is discussed later. Load distributions and deflection comparisons between figures 30 and 31 showed close agreement, validating the mechanical loading input of actuator arrangement 1. It should be noted however that to achieve this loading, a 29.6 inch stroke was required at the tip actuator. This stroke exceeded the 24 inch stroke capability of actuators used in similar tests in the structures lab. Also note that the additional connection length of the backstop to wing box transition structure was not included in the model. The inclusion of this structure would further increase actuator stroke requirements.

Figures 32, 33, and 34 show the effect of removing particular components of the applied baseline mechanical load. Figure 32 shows the effect of removing the leading edge actuator

force. Comparison to baseline results (figure 31) shows only slight variations in a small portion of the skin running loads. There was a greater variation of loading seen in the leading edge spar, which may or may not be of interest for overall test purposes.

Removal of the engine pylon load (figure 33) resulted in the same general distribution of internal loads as the baseline case. There was a slight increase in loading in the rear spar and skin element spanwise loads in the vicinity of the rear spar inboard of the engine pylon location. Also, tip deflection was increased about 0.5 inches for this load case.

Removal of the inertial loads (figure 34) also resulted in good agreement in internal load distribution as compared to the figure 31 baseline loading condition. The tip deflection increased only 0.2 inches. These results strengthen the case for not using inertial loads in the test simulation, if cost and complexity are major concerns. If a more accurate simulation of an actual flight condition were required, the inertial loading would have to be provided through a complex mechanical loading system.

The finite element results for loading using actuator arrangement 2 (see figure 24) are presented in figure 35. These results include tip loading, leading edge loading, engine pylon load and inertial loads, and are directly comparable to the results of figures 30 and 31. The results themselves are quite indistinguishable from those of figure 31 and verify the acceptability of this actuator arrangement. In addition, stroke requirements for this system were 23.8 inches at F1, 18.8 inches at F2, 16.3 inches at F3 and 11.4 inches at F4. The forces required at actuators F1 and F2 were 150,000 pounds each. An additional 14,400 pounds was required at F3 and an uplift load of -143,000 pounds was required at F4. The capability of being able to supply a large negative force, which implies pulling on floor beams which support the backstop structure, must be considered if this actuator loading system is chosen for implementation.

Backstop Attachment Structure

Backstop attachment structure was added to the model to investigate the local effects caused by applied thermal loading and interactions with the rigid backstop. Case 9, "Start of supersonic cruise, 57000 feet, Mach 2.4 3.75G (pull-up)," was chosen as a representative case which included thermal and mechanical loads. To simplify the analysis, it was assumed that the single actuator arrangement would be used to apply the loads to the test article. The backstop attachment structure was modeled as 0.5 inch thick 4130 steel plate, the same material and thickness used for the tip load introduction structure. The structure was added by extending the upper and lower wing skin surfaces and the internal webs a distance of 24 inches, as shown in figure 36.

The temperature distribution for the flight condition is nearly uniform, with approximately 300 degrees F on the top and bottom surfaces, and 150 degrees F on the internal structure. Figure 37 shows the upper skin temperature distribution for the flight load condition. For the test specimen analysis, a uniform temperature of 300 degrees F was applied to the wing box structure to simulate the effects of heat blankets. A linearly decreasing temperature varying from 300 degrees F at the wing box structure to 70 degrees F at the backstop was applied to the attachment structure. A similar distribution was applied to the tip load introduction structure.

Figure 36 shows the results for the flight load case with the complete set of thermal and mechanical loads included for Case 9. The flight boundary conditions supplied with the model were used for this analysis. Except for small areas of stress concentration, the spanwise running load varies between -14,000 and +1,000 pounds per inch. The shear running load varies from -24,000 and +6,000 pounds per inch. It is nearly uniform for the wing box, with small areas of concentration at connection points and around holes. Significantly larger forces are developed in the load introduction structure and the attachment structure, due to the relatively large increase in stiffness.

Figure 38 shows the results of applying the mechanical loads at room temperature to the laboratory model. In this simulation, the only mechanical load applied to the structure was the single 111,000 pound upward force at the tip actuator location. The root of the attachment

structure was pinned at the backstop. The figures show that the running load distribution was substantially the same as it was in the flight model. Due to the relatively large stiffness of the backstop attachment structure, the tip deflection only increased by about 0.5 inches over the deflection of a similar model that didn't include the backstop attachment structure.

Figure 39 shows the results of the thermal loading in addition to the mechanical load. The addition of the thermal loading altered the load distribution primarily in the vicinity of the connections to the attachment structure and the load introduction structure. The central area of the wing box, away from the boundaries, exhibited approximately the same internal load distribution. However, the plots in figure 39 indicate that the thermal expansion coefficient mismatch and the stiffness introduced into the chordwise direction by the stiff attachment structure cause increased load concentrations in the chordwise direction.

Figure 40 shows the results of using a titanium attachment structure as an alternative to the steel attachment structure. For this analysis the assumption was made that the wing box section would be manufactured with excess material which would be used as a transition structure to minimize the effects of the fixed boundary conditions. The attachment structure was modeled as uniform 0.108 inch thick titanium, instead of the 0.5 inch thick steel plate. The 0.108 inch thickness was chosen to match a typical thickness of plating on the upper skin. The results in figure 40 show that the spanwise running load distribution on the upper skin did not change substantially. However, the chordwise load distribution more closely matches the distribution for the flight load case. Shear running load distributions on the spar webs were not significantly affected.

Conclusions

A finite element model of an HSCT wing box test specimen was analyzed using the flight loads supplied with the model. The model was assessed in terms of mechanical load requirements for 12 load cases. Eight of these load cases, four subsonic maneuvers and four supersonic maneuvers were determined to be feasible test cases. One condition, a Mach .95 3.75G pull-up, was analyzed with a modified version of the finite element model to compare simulated laboratory test behavior to the behavior of the wing box subjected to predicted flight loads. Two actuator configurations were defined to supply a mechanical force system which would approximate the flight loading. The first configuration used only one actuator at the tip rib. This arrangement required moving the actuator load application point over a known range to simulate different flight conditions. Stroke requirements for this system were approximately 30 inches, with a maximum force requirement of 172,000 pounds. The second actuator configuration employed four actuators at the tip rib and reduced stroke requirements to approximately 24 inches and maximum force requirements to 150,000 pounds. Variable positioning of actuators for varying load conditions was not required for this setup. The four-actuator tip arrangement did, however, require a large uplift load on beams located in the floor which supports the Building 1148 backstop structure. If negative G maneuvers were to be simulated, both arrangements would require actuators which pull on these floor beams. Also for positive G maneuvers, the inclusion of engine pylon loads would require an actuator which would pull on the floor beams. Either of the two actuator arrangements would be able to simulate mechanical loads for the eight chosen flight conditions, provided that the floor beams are capable of resisting the uplift loads.

An attachment structure was added to the model to assess the local effects of the thermal loading and the interaction with the rigid backstop. The thermal loading increased the chordwise load concentrations in the vicinity of the backstop attachments. These concentrations could be reduced by manufacturing the test specimen with additional titanium wing box material which would act as a transition structure.

SECTION III

TEST FIXTURE DESIGN CONSIDERATIONS

Introduction

Load introduction fixtures, clamping hardware, and positioning of the wing component for test were investigated. The test component of the wing is shown in relation to the entire wing in figures 1 and 2. At the time of this study the construction methods and materials were not finalized. Therefore, an attachment system similar to an existing system (see figure 4) was copied. In this case the test component was a graphite/epoxy skin-stringer wing box subjected to a single point load. It was assumed that the HSCT test component will be similar except that the material will be titanium.

Attachment and Load Introduction Structure Concepts

The test component is shown attached to the backstop fixture at building 1148 in figure 41. A proposed interface bracket consists of a closed box section spliced to the test component at one end and attached at the other by bolting through a flange to t-bolt slots in the backstop. An extension added to the tip rib end consists of a boxed section attached with a skin splice joint. A hard point is provided on this extension to receive actuator loads. A torsional load introduction fitting is shown in figures 42 and 43 projecting from the leading edge with two actuators applying a torque load.

The test component is shown mounted approximately 10 feet above the floor in figure 42. This could be reduced to about 6 feet by using actuators shorter than those currently in use. The fore and aft location can vary several feet from center as shown. The width of the test component is about 17 feet and the width of the backstop is 30 feet.

The method of attaching adapter hardware by means of a splice plate would probably be feasible. One drawback of this approach, however, is that it does reduce the size of the structure being tested. The splice plates, which reinforce the edges of the structure, must be large in area due to the relatively high loads (e.g., 10,000 lb/inch in the skin). An additional consideration is the wing contour of the sample, which is not flat but conforms to a spanwise reduced airfoil shape at an angle to the direction of travel (X-axis). Approximate cross section cuts of the test component are shown in figure 44. The splices attaching the specimen will require three dimensional contour milling to mate with the skin.

Manufacturing Considerations

A better attachment scheme could be developed if hard points on the test component were defined and provided. These points will surely exist in the form of manufacturing joints, landing gear brackets, and engine mounts on the finished product. Testing requirements should be considered in the final design of the wing specimen.

REFERENCES

1. *Manual of Steel Construction*, 7th Edition, American Institute of Steel Construction , Inc., 1970
2. Winter, G., and Nilson, A.H., *Design of Concrete Structures*, John Wiley and Sons, Inc., 1974
3. Peck, R.B., Hanson, W.E., and Thornburn, T.H., *Foundation Engineering*, McGraw-Hill Book Company, 1972
4. DeAngelis, V.M., and Fields, R.A., *Techniques for Hot Structures Testing*, NASA TM 101727, 1990.

5. *Facility Systems for the Combined Loading Test System (COLTS), Building 1148*, Engineering Study Report, Vol I, Sverdrup Technology Incorporated, April 1992
6. *Facility Systems for the Combined Loading Test System (COLTS), Building 1148*, Engineering Study Report, Vol II, Sverdrup Technology Incorporated, April 1992

Table 1.- HSCT wing box finite element model summary

4520 nodes
626 CROD elements (tension compression 1-D members)
173 CBAR elements (bar elements with bending stiffness)
263 CTRIA3 triangular plate elements
4389 CQUAD4 quadrilateral plate elements
17 material properties*
47 rod element section properties
5 beam element section properties
94 plate element section properties

* There are 2 isotropic titanium materials (one a convenient duplicate of the other) and 15 properties specified by input stiffness matrices, all of which appear to be titanium, based on input densities and coefficients of expansion.

Table 2.- Loading conditions supplied with the finite element model

1) Seize limit
2) 9G Engine crash
3) 8G Vertical gust up
4) 8G Vertical gust down
5) Start of climb, Mach .5 3.75G (pull-up)
6) Start of climb, Mach .5 -1.5G (pushdown)
7) Start of subsonic cruise, Mach .95 3.75G (pull-up)
8) Start of subsonic cruise, Mach .95 -1.5g (pushdown)
9) Start of supersonic cruise, 57000 ft., Mach 2.4 3.75G (pull-up)
10) Start of supersonic cruise, 57000 ft., Mach 2.4 -1.5G (pushdown)
11) End of supersonic cruise, 65700 ft., Mach 2.4 3.75G (pull-up)
12) End of supersonic cruise, 65700 ft. Mach 2.4 -1.5G (pushdown)

Table 3.- Force summation for applied mechanical loading

Note: units are lbs for forces, and in-lbs for moments

	Tip rib			Leading Edge			Pylon
	Force	Bending Moment	Twisting Moment	Force	Bending Moment	Twisting Moment	Force
1) Seize Limit	28,700	2,360,000	-189,000	6,540	-169,000	-232,000	-9,300
2) Engine 9G crash	-280	114,000	133,000	-593	92,200	220,000	-120,000
3) 8g Up Vert Gust	29,100	2,210,000	-362,000	6,980	-212,000	-345,000	147,000
4) 8G Down Vert Gust	28,000	2,590,000	75,000	5,720	-66,600	22,100	-243,000
5) Start of Climb, Pullup	169,000	13,400,000	-8,290,000	43,500	-1,900,000	-2,630,000	-27,400
6) Start of Climb, Pushdown	-85,900	-7,100,000	4,260,000	-21,000	939,000	1,310,000	12,900
7) M .95 Subsonic Pullup	171,627	13,500,000	-8,390,000	42,300	-1,810,000	-2,500,000	-27,800
8) M .95 Subsonic Pushdown	-87,584	-7,180,000	4,330,000	-20,300	899,000	1,250,000	13,100
9) Mach 2.4 Pullup, 57000'	111,000	9,520,000	-2,260,000	26,700	-904,000	-1,270,000	-28,500
10) Mach 2.4 Pushdown 57000'	-72,700	-6,800,000	2,310,000	-16,500	694,000	985,000	15,500
11) Mach 2.4 Pullup 66000'	83,200	7,750,000	-1,230,000	16,700	-542,000	-753,000	-25,600
12) Mach 2.4 Pushdown 66000'	-54,400	-5,440,000	1,400,000	-10,700	435,000	618,000	13,800

	Internal Structure		
	Force, X	Force, Y	Force, Z
1) Seize Limit	855	667	-17,100
2) Engine 9G crash	335,000	-306,000	126,000
3) 8g Up Vert Gust	-471,000	474,000	-352,000
4) 8G Down Vert Gust	721,000	-641,000	402,000
5) Start of Climb, Pullup	1,820	1,330	-36,300
6) Start of Climb, Pushdown	-543	-378	10,700
7) M .95 Subsonic Pullup	1,610	1,180	-32,400
8) M .95 Subsonic Pushdown	-383	-276	8,520
9) Mach 2.4 Pullup, 57000'	1,640	1,230	-32,900
10) Mach 2.4 Pushdown 57000'	-247	-181	7,970
11) Mach 2.4 Pullup 66000'	2,120	1,620	-43,300
12) Mach 2.4 Pushdown 66000'	-632	-387	12,741

Table 4.- Required force location for applied mechanical loading

	Tip Load Actuator Location, cid=5		Leading Edge Load Actuator Location, cid=6	
	X, in	Y, in	X, in	Y, in
5) Start of Climb, Pullup	49	79	44	-60
6) Start of Climb, Pushdown	50	83	45	-62
7) M .95 Subsonic Pullup	49	79	43	-59
8) M .95 Subsonic Pushdown	49	82	44	-62
9) Mach 2.4 Pullup, 57000'	20	86	34	-48
10) Mach 2.4 Pushdown 57000'	32	94	42	-60
11) Mach 2.4 Pullup 66000'	15	93	32	-45
12) Mach 2.4 Pushdown 66000'	26	100	41	-58

Appendix A

Heating Power Requirements

Assume blanket size = 2' x 4' = 8 ft^2

Test specimen is approx 2 x 16' x 18' = 576 ft^2

No. of blankets req'd = 576 ft^2/(8 ft^2/blanket) = 72 blankets

Power Required for HSCT Wing Box

Test Temperature = 350 °F

$Q_{wing} = mc_p\Delta T$

T_{room} = 72 °F

T_{final} = 350 °F => ΔT = 278 °F

W_{wing} ~ 3600 lbs

c_p = 0.126 BTU/lb-°F for titanium

Q_{wing} = 3600 lbs * 0.126 BTU/lb-°F * 278 °F * 3.412 BTU/Watt-hr

= 37 KW-hrs

Heat losses due to convection, Q_L => 81.50 kW-hr

wing side surface	2.79 kW-hr
wing top surface	34.77 kW-hr
wing bottom surface	43.94 kW-hr

Heat Required for 1hr Startup to 350 °F (with 10% safety factor):

$Q_{start} = (Q_{wing} + 2/3Q_L) * (1.10) = 120$ kW

Total Heat required = Losses + Unknown factors:

Q_{req} = unknown factor $*Q_L * (1.10) = 240$ kW

120 kW < Q_{req} < 240 kW (or .250 MW min required)

(Note: unknown factor of 2 is used to estimate effects of heat loss mechanisms not explicitly accounted for in calculations.)

Heat Loss to Backstop Calculations

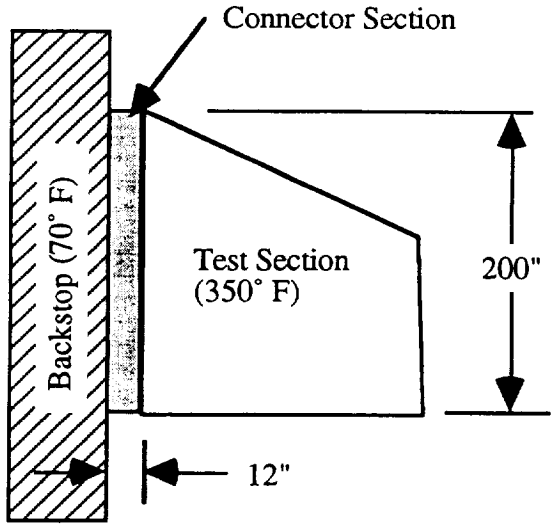

1) Connector Section Preliminary Sizing
   - Assume 12" connector section length
   - From finite element analysis, Running loads for 2.5G maneuver are 12,000 lb/in. at the wing root.
   - Assume a 0.50" thick attachment structure (s≈24 ksi).
2) Heat Loss to Backstop through Connector Section
   - Assume mild steel thermal properties. (k=30 Btu/ft-hr-°F)
   - Total running length of connector perimeter and webs - 440 inches.
   - For worst case heat flow, assume test section at 350° F and backstop at 70° F.
   - The heat loss through the connector is then

$$Q = \frac{kA}{l}\Delta T = \frac{(30\ \text{Btu/ft-hr-°F})(440\text{in.})(0.50\text{in.})}{(12\ \text{in.})(12\text{in./1ft.})}\ (350°\ \text{F} - 70°\ \text{F})$$

$$Q = 12{,}800\ \text{Btu/hr} = 3760\ \text{Watts}$$

This heat loss total is small compared to the other heat blanket losses and also to the amount of heat required to raise the wing temperature for 70° to 350° F.

Appendix B

Floor Weight Calculations

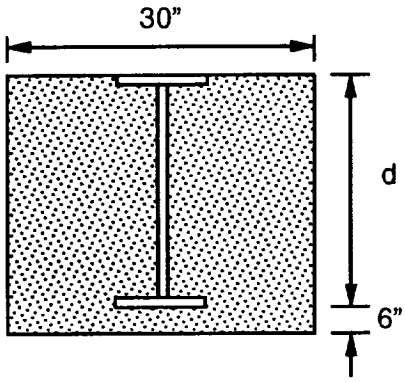

concrete unit weight:

$$\frac{0.150^{k}}{ft^3}\frac{1\ ft^3}{1728\ in^3} = 0.868e-4\ \frac{k}{in^3}$$

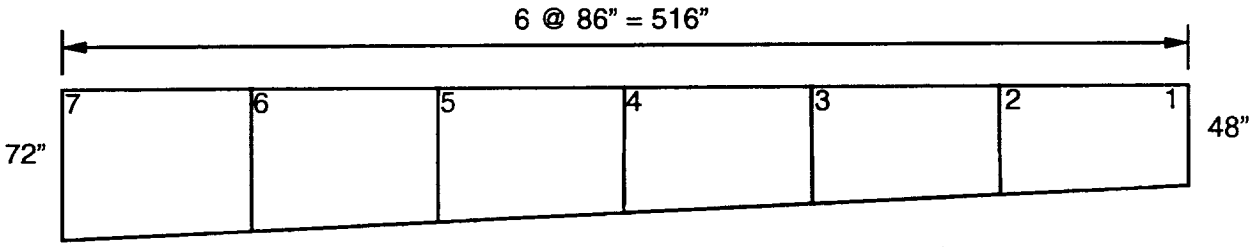

load at each station = 30 x d x 86 x 0.86e-4

estimate of total slab weight: $(30')(92')(4.5')\left(0.150\frac{k}{ft^3}\right) = 1863^{k}$

Column Weight

dead weight of column: $\left[2\,(16.125")(1.875") + (56.25")(1.25")\right](240")\left(.283e-3\frac{k}{in^3}\right) = 8.9^{k}$

dead weight of top plate: $(30")(60")(1.5")\left(.283e-3\frac{k}{in^3}\right) = 0.76^{k}$

dead weight of mounting plates (per column): $2\,(30")(7")(120")\left(.283e-3\frac{k}{in^3}\right) = 14.3^{k}$

Total weight at bottom of each column = 23.96^{k}

Total weight of columns and mounting plates = 13 columns x 23.96^{k} / column = 311.5^{k}

Appendix C

Constraint Force Summation on Leading Edge for the HSR Wing Box Model

Forces and moments summed at origin of coordinate system 6, see figure 22
Force in lbs, Moments in inch-lbs

	X	Y	Z
Loadcase 1) Seize Limit			
Applied Translational Constraint Forces	728	-1,330	6,535
Moments from Applied Translational Constraint Forces	-225,379	-155,192	-8,159
Applied Rotational Forces	-6,383	-13,964	-1,110
Total Force Summation	728	-1,330	6,535
Total Moment Summation	-231,762	-169,156	-9,269
Loadcase 2) Engine 9G crash			
Applied Translational Constraint Forces	-170	667	-593
Moments from Applied Translational Constraint Forces	219,929	118,142	23,518
Applied Rotational Forces	322	-25,907	4,590
Total Force Summation	-170	667	-593
Total Moment Summation	220,251	92,235	28,108
Loadcase 3) 8G vert gust up			
Applied Translational Constraint Forces	856	-1,790	6,980
Moments from Applied Translational Constraint Forces	-338,309	-213,213	-25,549
Applied Rotational Forces	-6,443	736	-4,866
Total Force Summation	856	-1,790	6,980
Total Moment Summation	-344,752	-212,477	-30,415
Loadcase 4) 8G vert gust down			
Applied Translational Constraint Forces	483	-403	5,724
Moments from Applied Translational Constraint Forces	28,847	-21,426	-24,467
Applied Rotational Forces	-6,730	-45,185	5,966
Total Force Summation	483	-403	5,724
Total Moment Summation	22,117	-66,611	-18,501
Loadcase 5) SOC pull-up			
Applied Translational Constraint Forces	3,751	-6,215	43,523
Moments from Applied Translational Constraint Forces	-2,480,750	-1,655,660	-82,429
Applied Rotational Forces	-146,850	-242,755	5,963
Total Force Summation	3,751	-6,215	43,523
Total Moment Summation	-2,627,600	-1,898,415	-76,467
Loadcase 6) SOC push-down			
Applied Translational Constraint Forces	-1,975	3,659	-20,874
Moments from Applied Translational Constraint Forces	1,231,830	819,035	42,215
Applied Rotational Forces	75,514	120,357	-2,267
Total Force Summation	-1,975	3,659	-20,874
Total Moment Summation	1,307,344	939,392	39,948

Loadcase 7) Subsonic pull-up			
Applied Translational Constraint Forces	3,864	-6,630	42,308
Moments from Applied Translational Constraint Forces	-2,360,790	-1,579,510	-79,080
Applied Rotational Forces	-137,772	-227,776	4,262
Total Force Summation	3,864	-6,630	42,308
Total Moment Summation	-2,498,562	-1,807,286	-74,818
Loadcase 8) Subsonic Push-down			
Applied Translational Constraint Forces	-2,044	3,906	-20,346
Moments from Applied Translational Constraint Forces	1,178,770	785,292	40,760
Applied Rotational Forces	71,604	113,640	-1,516
Total Force Summation	-2,044	3,906	-20,346
Total Moment Summation	1,250,374	898,932	39,244
Loadcase 9) Supersonic Pull-up 57000'			
Applied Translational Constraint Forces	2,726	-4,815	26,678
Moments from Applied Translational Constraint Forces	-1,207,000	-808,658	-43,861
Applied Rotational Forces	-60,734	-95,010	257
Total Force Summation	2,726	-4,815	26,678
Total Moment Summation	-1,267,734	-903,668	-43,604
loadcase 10) Supersonic push-down 57000'			
Applied Translational Constraint Forces	-1,584	2,759	-16,517
Moments from Applied Translational Constraint Forces	926,759	611,404	34,914
Applied Rotational Forces	58,556	82,620	-3,006
Total Force Summation	-1,584	2,759	-16,517
Total Moment Summation	985,315	694,024	31,908
Loadcase 11) Supersonic Pull-up, 66000'			
Applied Translational Constraint Forces	1,799	-3,133	16,747
Moments from Applied Translational Constraint Forces	-720,823	-486,918	-27,895
Applied Rotational Forces	-32,506	-55,222	22
Total Force Summation	1,799	-3,133	16,747
Total Moment Summation	-753,329	-542,140	-27,873
Loadcase 12) Supersonic push-down, 66000'			
Applied Translational Constraint Forces	-1,069	1,761	-10,692
Moments from Applied Translational Constraint Forces	581,474	384,191	22,395
Applied Rotational Forces	36,752	51,196	-2,393
Total Force Summation	-1,069	1,761	-10,692
Total Moment Summation	618,226	435,387	20,002
Max Force Sum, all load cases	3,864	3,906	43,523
Max Moment Sum, all load cases	1,307,344	939,392	39,948
Min Force Sum, all load cases	-2,044	-6,630	-20,874
Min Moment Sum, all load cases	-2,627,600	-1,898,415	-76,467

Constraint Force Summation on Internal Structure for the HSR Wing Box Model

Forces and moments summed at origin of coordinate system 5, see figure 22
Force in lbs, Moments in inch-lbs

	X	Y	Z
Loadcase 1) Seize Limit			
Applied Translational Constraint Forces	855	667	-17124
Moments from Applied Translational Constraint Forces	2.62E+07	1565	-5.52E+06
Applied Rotational Forces	0	0	0
Total Force Summation	855	667	-17,124
Total Moment Summation	2,620,000	1,565	-552,024
Loadcase 2) Engine 9G crash			
Applied Translational Constraint Forces	334603	-306068	125739
Moments from Applied Translational Constraint Forces	-4397.66	-951.995	1.72031
Applied Rotational Forces	0	0	0
Total Force Summation	334,603	-306,068	125,739
Total Moment Summation	-4,398	-952	2
Loadcase 3) 8G vert gust up			
Applied Translational Constraint Forces	-470738	473528	-352170
Moments from Applied Translational Constraint Forces	5.52E+08	6.23E+07	-6.30E+08
Applied Rotational Forces	0	0	0
Total Force Summation	-470,738	473,528	-352,170
Total Moment Summation	55,160,000	6,230,000	-63,000,000
Loadcase 4) 8G vert gust down			
Applied Translational Constraint Forces	720976	-641059	402151
Moments from Applied Translational Constraint Forces	-6.36E+08	-1.21E+08	9.18E+08
Applied Rotational Forces	0	0	0
Total Force Summation	720,976	-641,059	402,151
Total Moment Summation	-63,600,000	-12,100,000	91,800,000
Loadcase 5) SOC pull-up			
Applied Translational Constraint Forces	1822	1330	-36335
Moments from Applied Translational Constraint Forces	6.08E+07	325719	-1.32E+07
Applied Rotational Forces	0	0	0
Total Force Summation	1,822	1,330	-36,335
Total Moment Summation	6,080,000	325,719	-1,320,000
Loadcase 6) SOC push-down			
Applied Translational Constraint Forces	-543	-378	10690
Moments from Applied Translational Constraint Forces	-2.15E+07	-339154	711573
Applied Rotational Forces	0	0	0
Total Force Summation	-543	-378	10,690
Total Moment Summation	-2,150,000	-339,154	711,573

Loadcase 7) Subsonic pull-up			
Applied Translational Constraint Forces	1609	1183	-32359
Moments from Applied Translational Constraint Forces	5.74E+07	375115	-1.35E+07
Applied Rotational Forces	0	0	0
Total Force Summation	1,609	1,183	-32,359
Total Moment Summation	5,740,000	375,115	-1,350,000
Loadcase 8) Subsonic Push-down			
Applied Translational Constraint Forces	-383	-276	8524
Moments from Applied Translational Constraint Forces	-1.97E+07	-370434	735737
Applied Rotational Forces	0	0	0
Total Force Summation	-383	-276	8,524
Total Moment Summation	-1,970,000	-370,434	735,737
Loadcase 9) Supersonic Pull-up 57000'			
Applied Translational Constraint Forces	1637	1229	-32907
Moments from Applied Translational Constraint Forces	5.78E+07	508106	-1.12E+07
Applied Rotational Forces	0	0	0
Total Force Summation	1,637	1,229	-32,907
Total Moment Summation	5,780,000	508,106	-1,120,000
loadcase 10) Supersonic push-down 57000'			
Applied Translational Constraint Forces	-247	-181	7966
Moments from Applied Translational Constraint Forces	-1.92E+07	-626727	1.10E+06
Applied Rotational Forces	0	0	0
Total Force Summation	-247	-181	7,966
Total Moment Summation	-1,920,000	-626,727	110,374
Loadcase 11) Supersonic Pull-up, 66000'			
Applied Translational Constraint Forces	2115	1623	-43315
Moments from Applied Translational Constraint Forces	6.62E+07	248985	-8.27E+06
Applied Rotational Forces	0	0	0
Total Force Summation	2,115	1,623	-43,315
Total Moment Summation	6,620,000	248,985	-827,134
Loadcase 12) Supersonic push-down, 66000'			
Applied Translational Constraint Forces	-632	-387	12741
Moments from Applied Translational Constraint Forces	-2.29E+07	-433355	-6.55E+05
Applied Rotational Forces	0	0	0
Total Force Summation	-632	-387	12,741
Total Moment Summation	-2,290,000	-433,355	-65,474
Max Force Sum	720,976	473,528	402,151
Max Moment Sum	55,160,000	6,230,000	91,800,000
Min Force Sum	-470,738	-641,059	-352,170
Min Moment Sum	-63,600,000	-12,100,000	-63,000,000

Constraint Force Summation on Trailing Edge Pylon for the HSR Wing Box Model

Forces and moments summed at origin of coordinate system 9, see figure 22
Force in lbs, Moments in inch-lbs

	X	Y	Z
Loadcase 1) Seize Limit			
Applied Translational Constraint Forces	0	-15	-9,297
Moments from Applied Translational Constraint Forces	-335	-291	0
Applied Rotational Forces	0	0	0
Total Force Summation	0	-15	-9,297
Total Moment Summation	-335	-291	0
Loadcase 2) Engine 9G crash			
Applied Translational Constraint Forces	-4	-199	-120,060
Moments from Applied Translational Constraint Forces	-4,398	-952	2
Applied Rotational Forces	0	0	0
Total Force Summation	-4	-199	-120,060
Total Moment Summation	-4,398	-952	2
Loadcase 3) 8G vert gust up			
Applied Translational Constraint Forces	5	243	146,623
Moments from Applied Translational Constraint Forces	5,377	945	-2
Applied Rotational Forces	0	0	0
Total Force Summation	5	243	146,623
Total Moment Summation	5,377	945	-2
Loadcase 4) 8G vert gust down			
Applied Translational Constraint Forces	-8	-403	-242,976
Moments from Applied Translational Constraint Forces	-8,894	-2,144	4
Applied Rotational Forces	0	0	0
Total Force Summation	-8	-403	-242,976
Total Moment Summation	-8,894	-2,144	4
Loadcase 5) SOC pull-up			
Applied Translational Constraint Forces	_	-46	-27,408
Moments from Applied Translational Constraint Forces	-989	-762	1
Applied Rotational Forces	0	0	0
Total Force Summation	_	-46	-27,408
Total Moment Summation	-989	-762	1
Loadcase 6) SOC push-down			
Applied Translational Constraint Forces	0	21	12,907
Moments from Applied Translational Constraint Forces	467	320	_
Applied Rotational Forces	0	0	0
Total Force Summation	0	21	12,907
Total Moment Summation	467	320	_

Loadcase 7) Subsonic pull-up			
Applied Translational Constraint Forces	_	-46	-27,798
Moments from Applied Translational Constraint Forces	-1,003	-765	1
Applied Rotational Forces	0	0	0
Total Force Summation	_	-46	-27,798
Total Moment Summation	-1,003	-765	1
Loadcase 8) Subsonic Push-down			
Applied Translational Constraint Forces	0	22	13,122
Moments from Applied Translational Constraint Forces	475	322	_
Applied Rotational Forces	0	0	0
Total Force Summation	0	22	13,122
Total Moment Summation	475	322	_
Loadcase 9) Supersonic Pull-up 57000'			
Applied Translational Constraint Forces	0	-47	-28,533
Moments from Applied Translational Constraint Forces	-1,031	-770	1
Applied Rotational Forces	0	0	0
Total Force Summation	0	-47	-28,533
Total Moment Summation	-1,031	-770	1
loadcase 10) Supersonic push-down 57000'			
Applied Translational Constraint Forces	0	26	15,505
Moments from Applied Translational Constraint Forces	562	341	0
Applied Rotational Forces	0	0	0
Total Force Summation	0	26	15,505
Total Moment Summation	562	341	0
Loadcase 11) Supersonic Pull-up, 66000'			
Applied Translational Constraint Forces	0	-43	-25,637
Moments from Applied Translational Constraint Forces	-924	-747	1
Applied Rotational Forces	0	0	0
Total Force Summation	0	-43	-25,637
Total Moment Summation	-924	-747	1
Loadcase 12) Supersonic push-down, 66000'			
Applied Translational Constraint Forces	0	23	13,802
Moments from Applied Translational Constraint Forces	500	327	0
Applied Rotational Forces	0	0	0
Total Force Summation	0	23	13,802
Total Moment Summation	500	327	0
Max Force Sum	5	243	146,623
Max Moment Sum	5,377	945	4
Min Force Sum	-8	-403	-242,976
Min Moment Sum	-8,894	-2,144	-2

Constraint Force Summation on Tip Rib for the HSR Wing Box Model

Forces and moments summed at origin of coordinate system 5, see figure 22
Force in lbs, Moments in inch-lbs

	X	Y	Z
Loadcase 1) Seize Limit			
Applied Translational Constraint Forces	-841	-10	28,681
Moments from Applied Translational Constraint Forces	2,340,000	-189,121	44,218
Applied Rotational Forces	18,881	-296	-1,743
Total Force Summation	-841	-10	28,681
Total Moment Summation	2,358,881	-189,417	42,475
Loadcase 2) Engine 9G crash			
Applied Translational Constraint Forces	12	24	-280
Moments from Applied Translational Constraint Forces	111,184	143,366	29,500
Applied Rotational Forces	3,101	-9,959	691
Total Force Summation	12	24	-280
Total Moment Summation	114,285	133,407	30,190
Loadcase 3) 8G vert gust up			
Applied Translational Constraint Forces	-874	-14	29,119
Moments from Applied Translational Constraint Forces	2,200,000	-372,789	13,094
Applied Rotational Forces	12,815	11,146	-2,470
Total Force Summation	-874	-14	29,119
Total Moment Summation	2,212,815	-361,643	10,624
Loadcase 4) 8G vert gust down			
Applied Translational Constraint Forces	-795	2	28,030
Moments from Applied Translational Constraint Forces	2,560,000	92,811	95,174
Applied Rotational Forces	27,382	-17,859	-582
Total Force Summation	-795	2	28,030
Total Moment Summation	2,587,382	74,952	94,592
Loadcase 5) SOC pull-up			
Applied Translational Constraint Forces	-5,572	-657	169,158
Moments from Applied Translational Constraint Forces	13,370,600	-8,233,080	77,352
Applied Rotational Forces	61,002	-57,149	-2,174
Total Force Summation	-5,572	-657	169,158
Total Moment Summation	13,431,602	-8,290,229	75,178
Loadcase 6) SOC push-down			
Applied Translational Constraint Forces	2,850	486	-85,935
Moments from Applied Translational Constraint Forces	-7,074,210	4,229,430	-41,148
Applied Rotational Forces	-34,219	26,712	1,198
Total Force Summation	2,850	486	-85,935
Total Moment Summation	-7,108,429	4,256,142	-39,950

Loadcase 7) Subsonic pull-up			
Applied Translational Constraint Forces	-5,570	-811	171,627
Moments from Applied Translational Constraint Forces	13,477,000	-8,334,950	75,959
Applied Rotational Forces	64,244	-53,466	-2,191
Total Force Summation	-5,570	-811	171,627
Total Moment Summation	13,541,244	-8,388,416	73,768
Loadcase 8) Subsonic Push-down			
Applied Translational Constraint Forces	2,835	579	-87,584
Moments from Applied Translational Constraint Forces	-7,147,340	4,307,060	-38,493
Applied Rotational Forces	-35,928	24,951	1,226
Total Force Summation	2,835	579	-87,584
Total Moment Summation	-7,183,268	4,332,011	-37,267
Loadcase 9) Supersonic Pull-up 57000'			
Applied Translational Constraint Forces	-3,425	-647	111,425
Moments from Applied Translational Constraint Forces	9,450,000	-2,250,000	132,262
Applied Rotational Forces	65,858	-12,921	-3,147
Total Force Summation	-3,425	-647	111,425
Total Moment Summation	9,515,858	-2,262,921	129,115
loadcase 10) Supersonic push-down 57000'			
Applied Translational Constraint Forces	2,260	686	-72,672
Moments from Applied Translational Constraint Forces	-6,750,000	2,300,000	-62,673
Applied Rotational Forces	-43,340	11,550	61
Total Force Summation	2,260	686	-72,672
Total Moment Summation	-6,793,340	2,311,550	-62,612
Loadcase 11) Supersonic Pull-up, 66000'			
Applied Translational Constraint Forces	-2,418	-366	83,196
Moments from Applied Translational Constraint Forces	7,690,000	-1,230,000	105,023
Applied Rotational Forces	59,838	-309	-2,798
Total Force Summation	-2,418	-366	83,196
Total Moment Summation	7,749,838	-1,230,309	102,225
Loadcase 12) Supersonic push-down, 66000'			
Applied Translational Constraint Forces	1,600	557	-54,435
Moments from Applied Translational Constraint Forces	-5,400,000	1,400,000	-52,342
Applied Rotational Forces	-38,801	3,466	-227
Total Force Summation	1,600	557	-54,435
Total Moment Summation	-5,438,801	1,403,466	-52,569
Max F	2,850	686	171,627
Max Moment Sum	13,541,244	4,332,011	129,115
Min F	-5,572	-811	-87,584
Min Moment Sum	-7,183,268	-8,388,416	-62,612

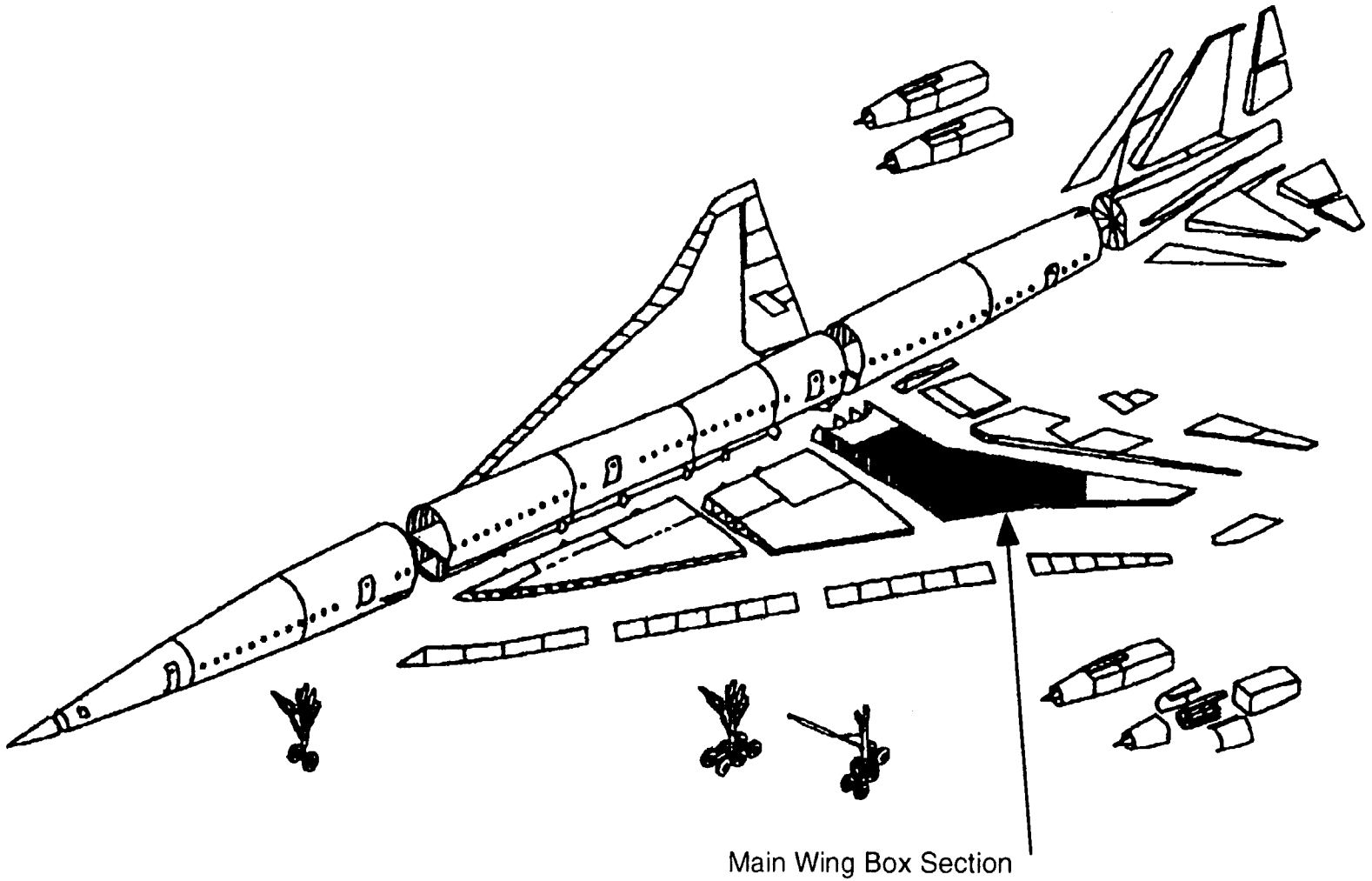

Figure 1.- McDonnell Douglas HSCT concept

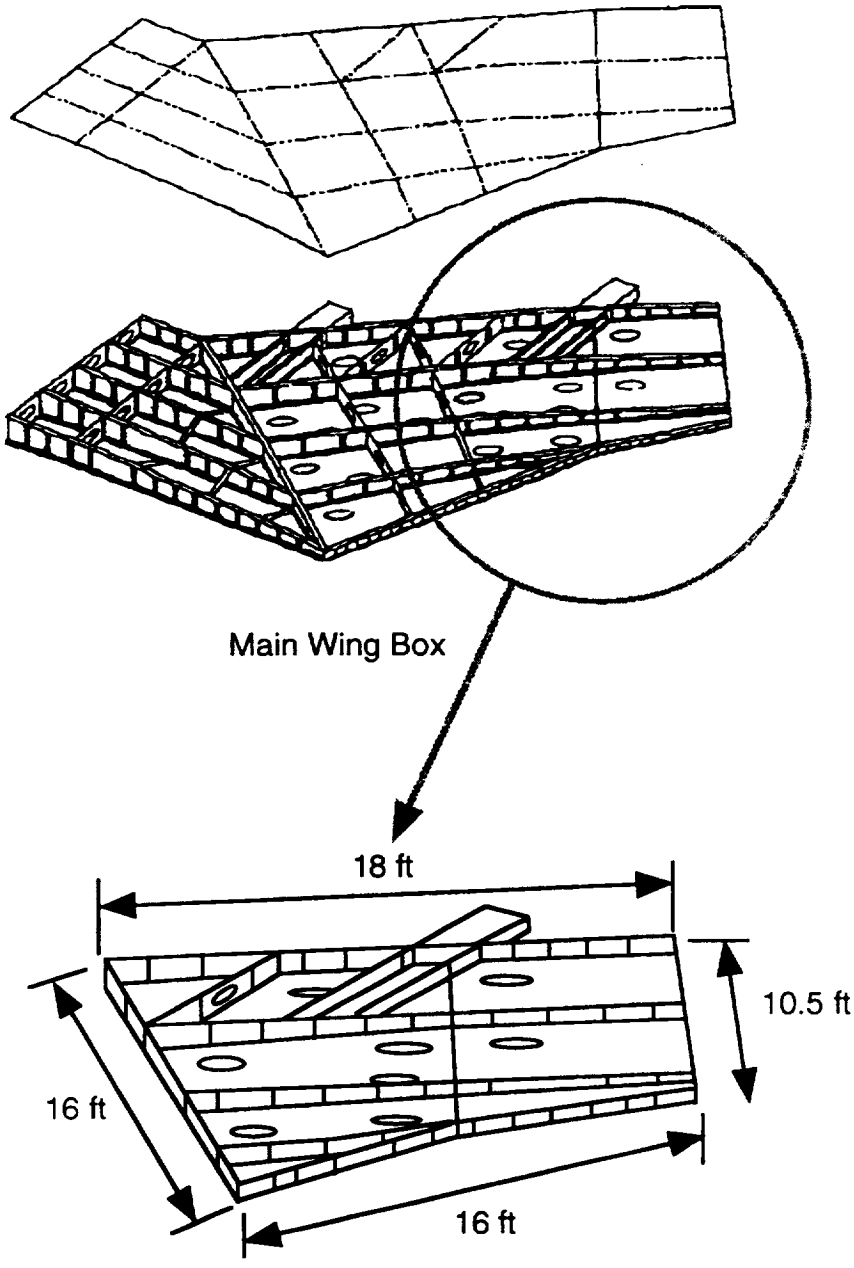

Figure 2.- Wing box test specimen with approximate dimensions

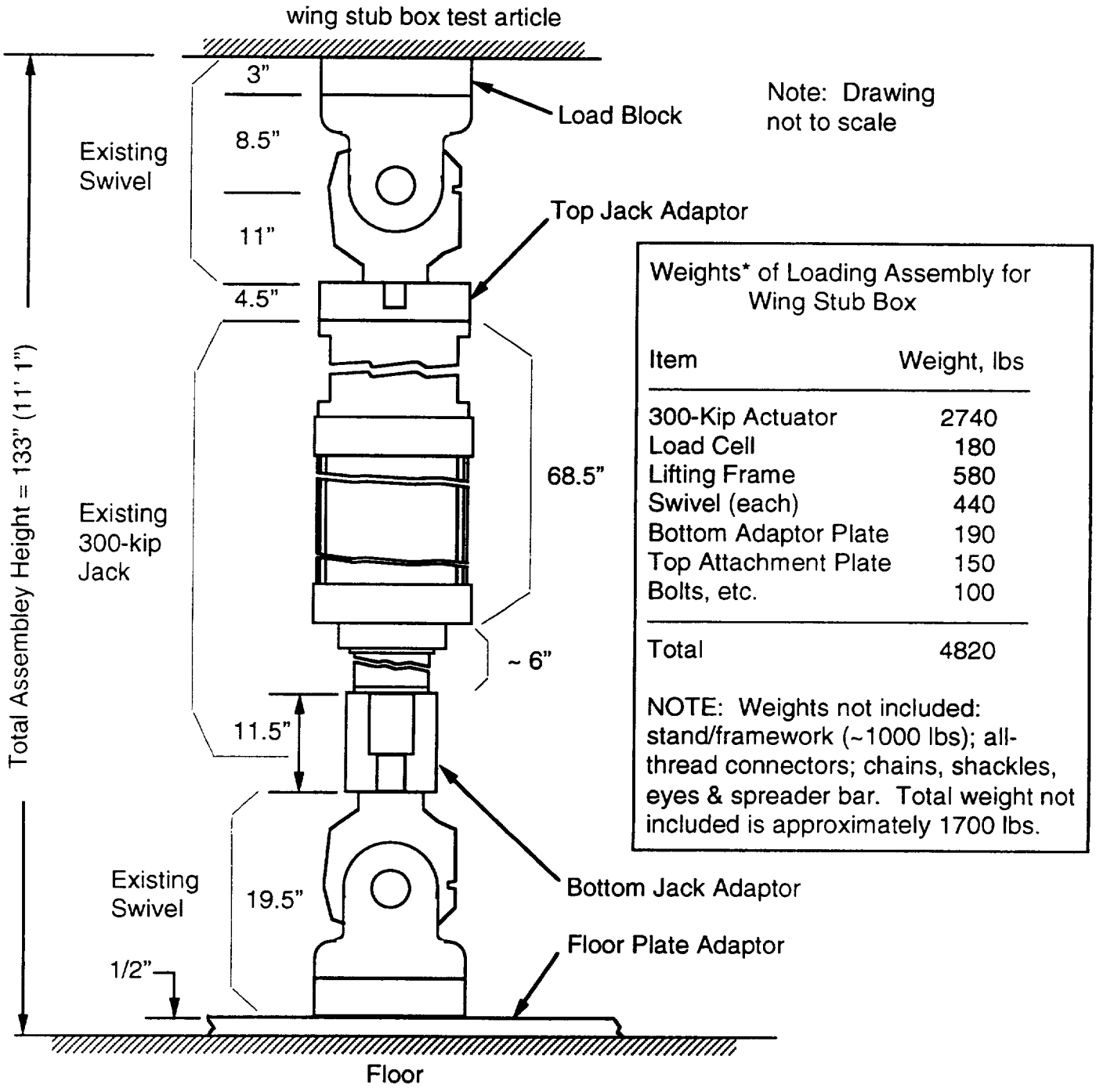

Weights* of Loading Assembly for Wing Stub Box

Item	Weight, lbs
300-Kip Actuator	2740
Load Cell	180
Lifting Frame	580
Swivel (each)	440
Bottom Adaptor Plate	190
Top Attachment Plate	150
Bolts, etc.	100
Total	4820

NOTE: Weights not included: stand/framework (~1000 lbs); all-thread connectors; chains, shackles, eyes & spreader bar. Total weight not included is approximately 1700 lbs.

Figure 3.- Wing stub box loading assembly

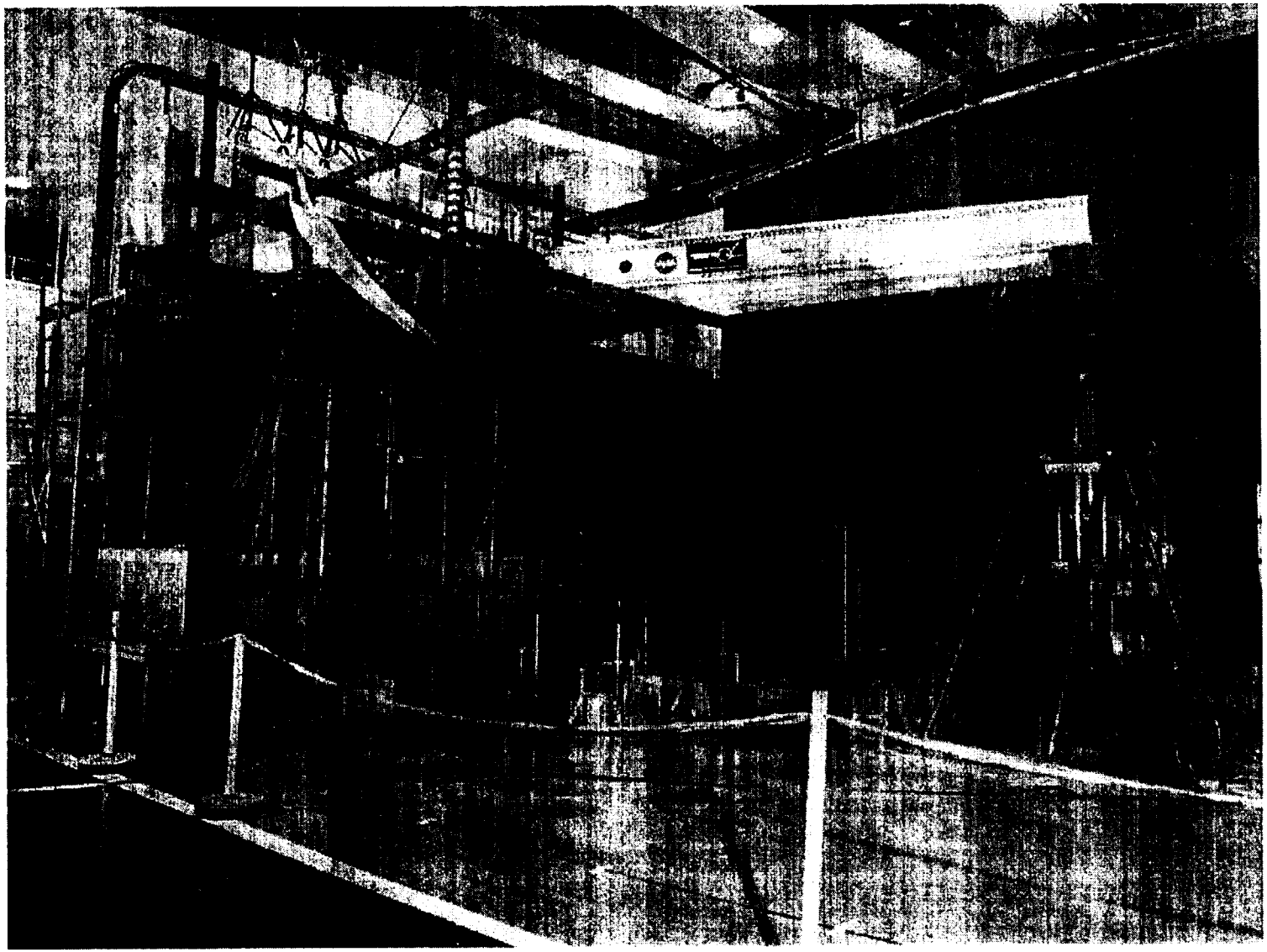

Figure 4.- Wing stub box test

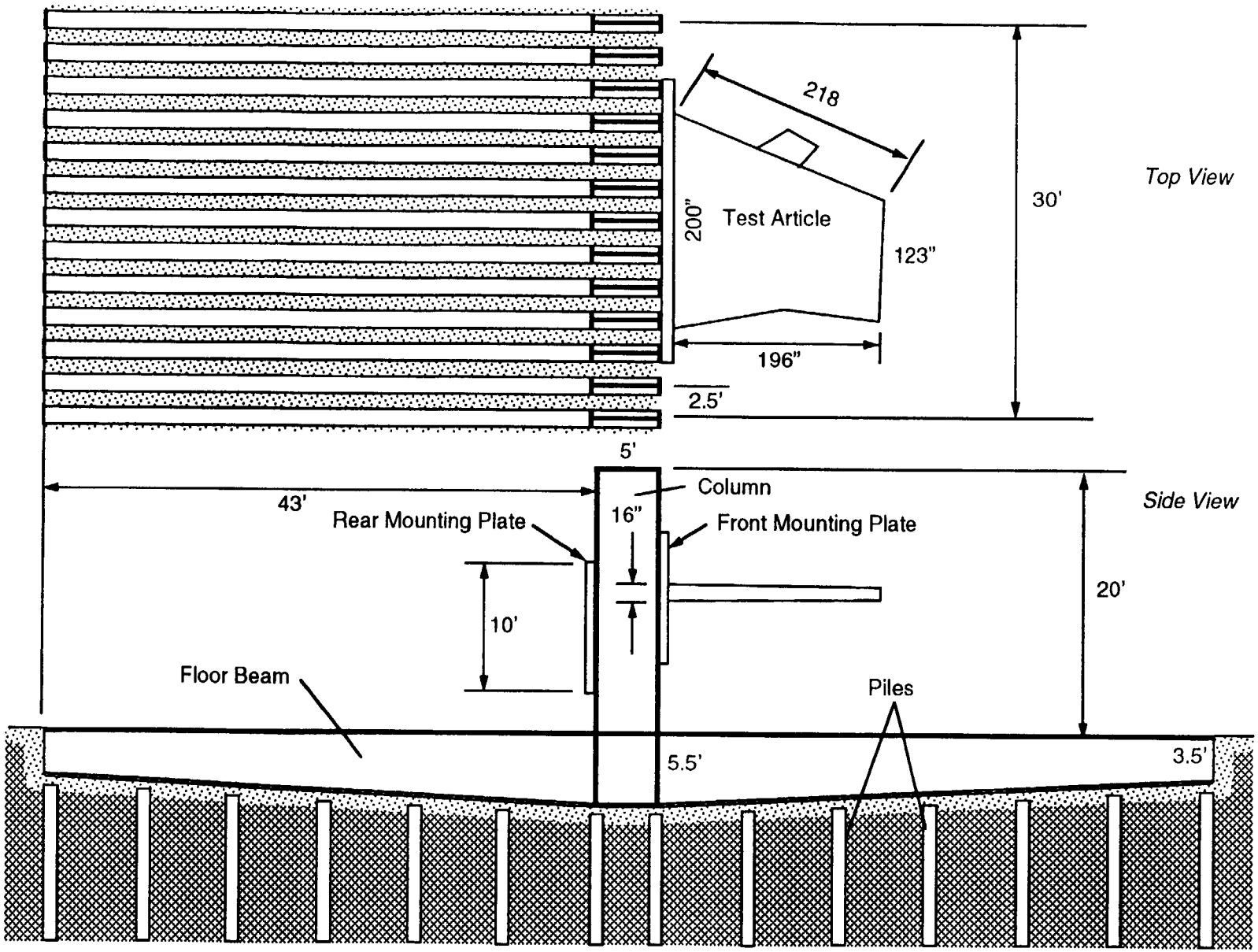

Figure 5-. Backstop/floor support structure

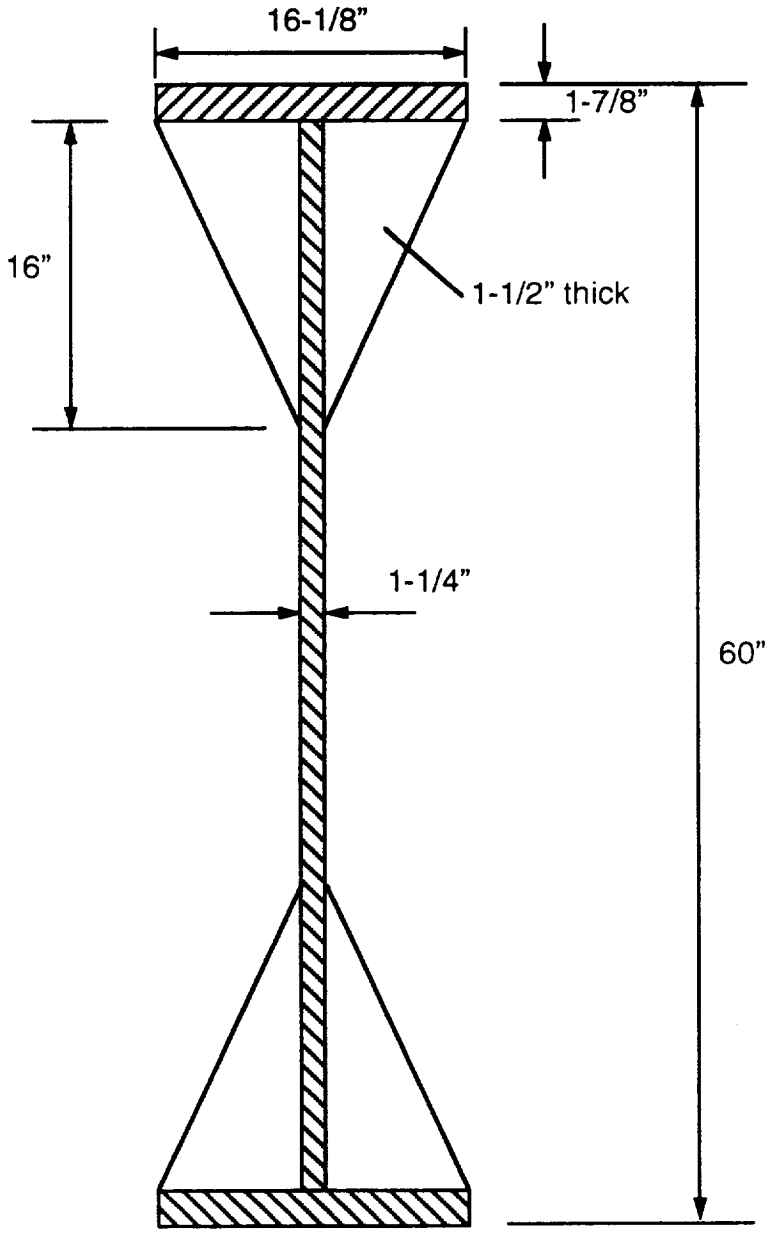

Backstop Column

Figure 6.- Backstop column

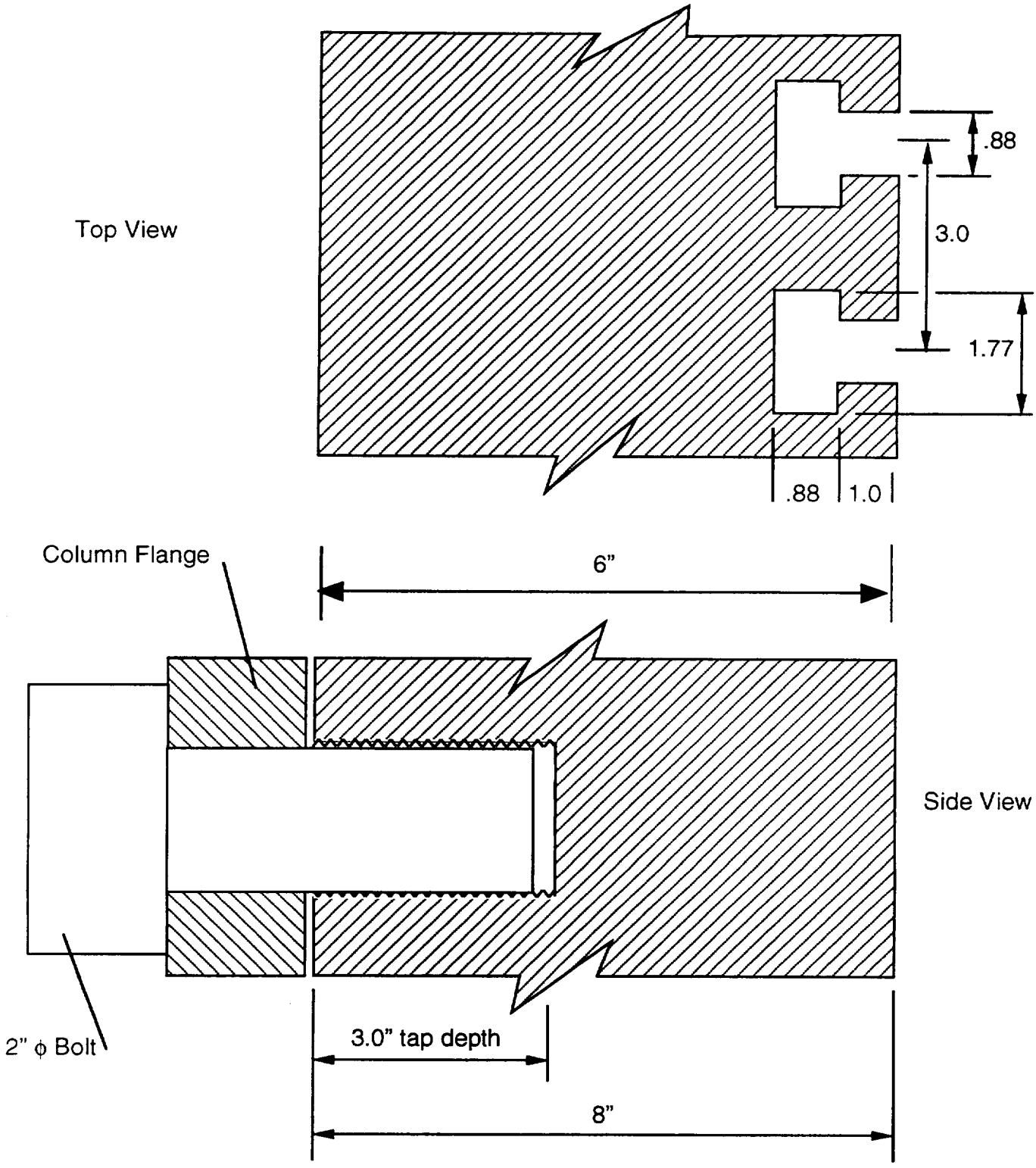

Figure 7.- Mounting plate

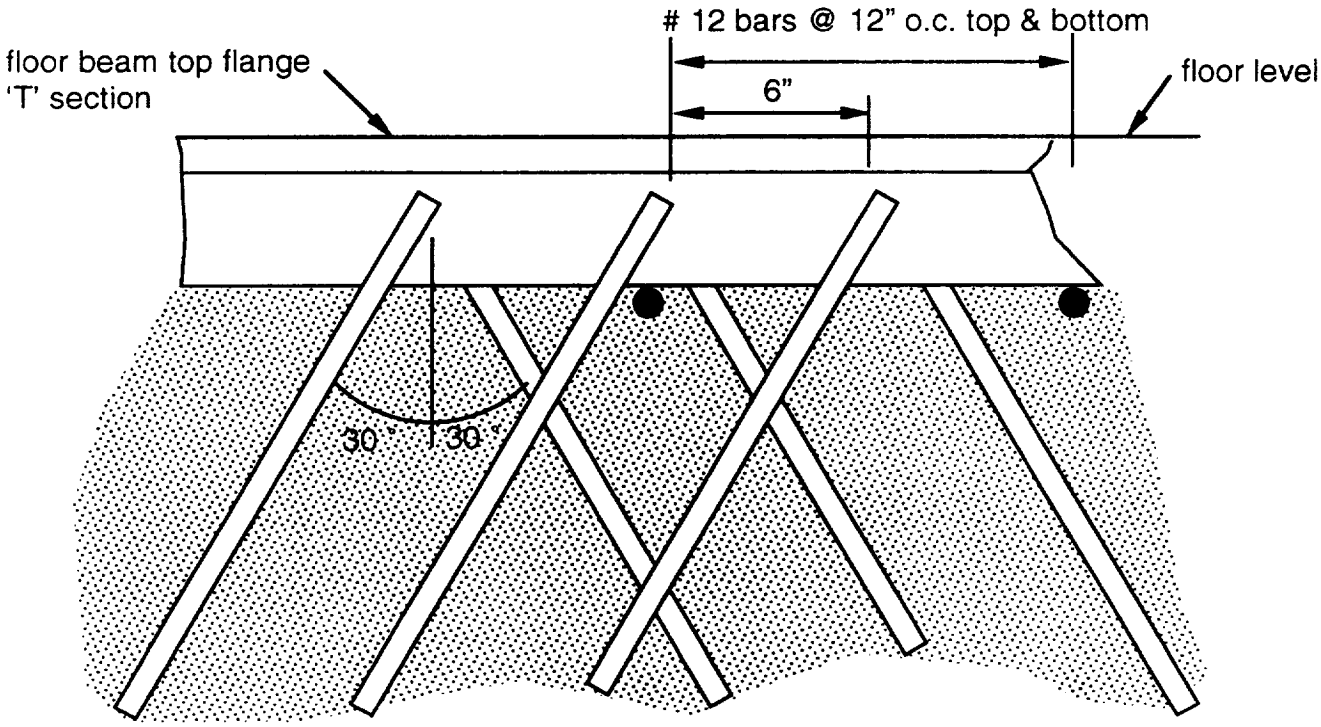

NOTE: The web of the floor beam is formed by diagonal bars welded to the top and bottom flanges and encased in concrete.

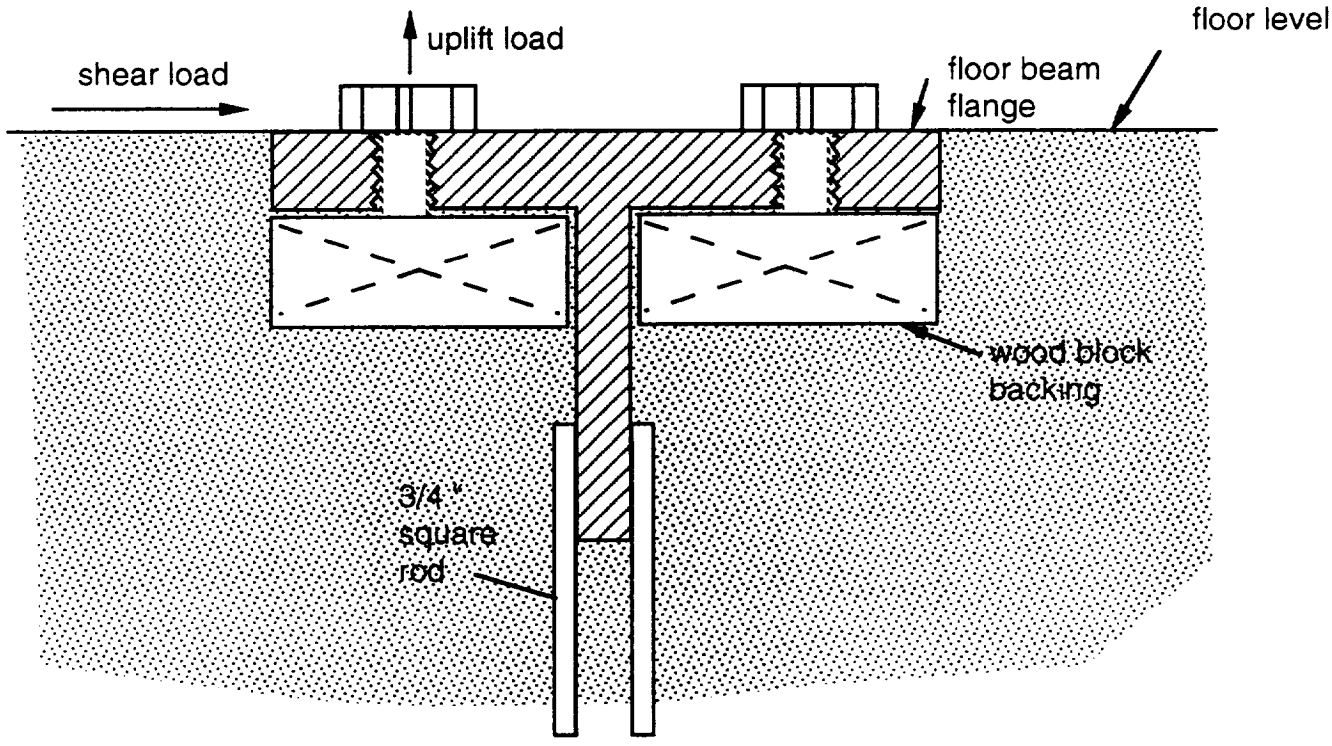

Figure 8.- Floor beams

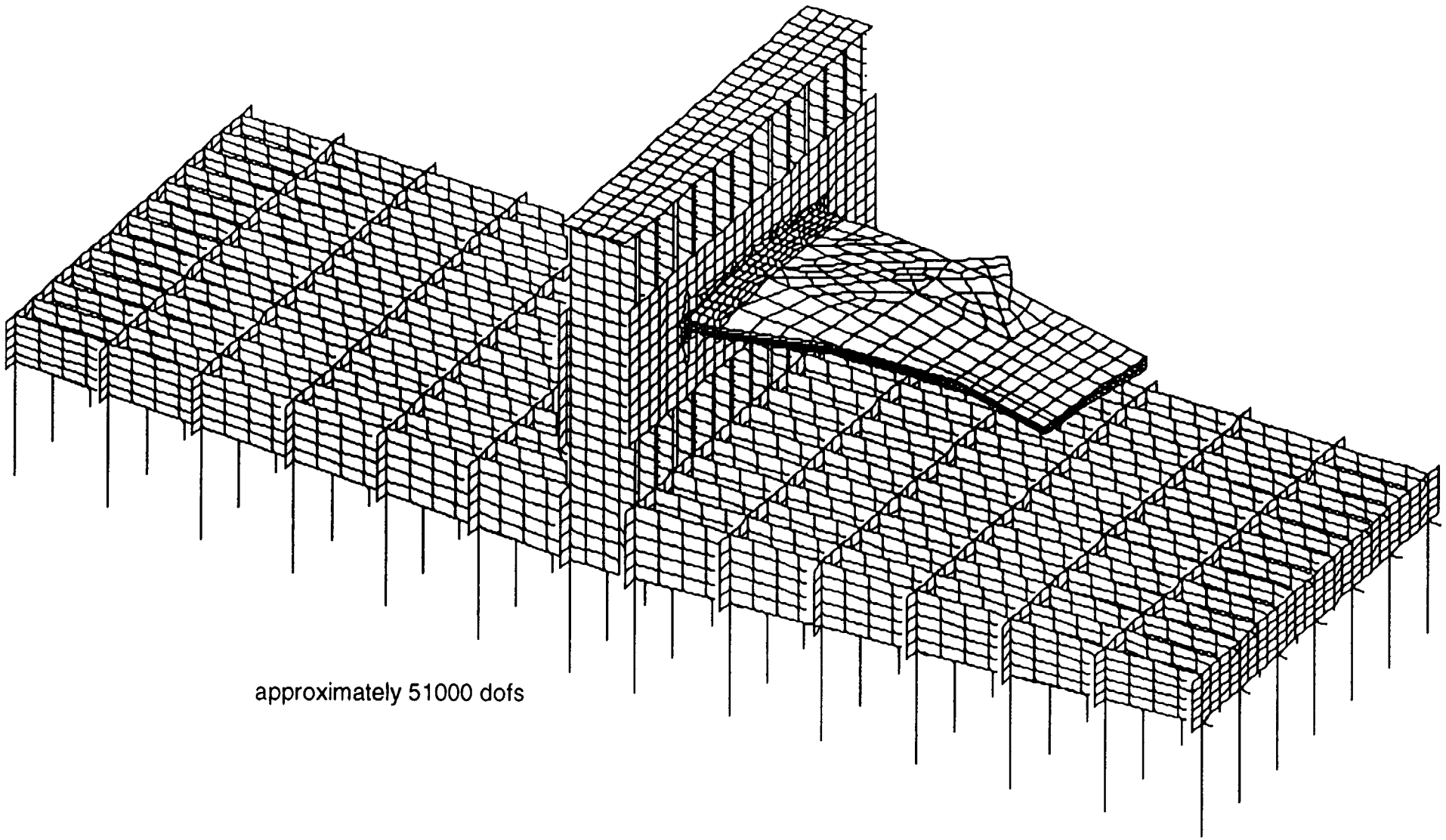

Figure 9.- Building 1148 backstop with proposed HSR wing box

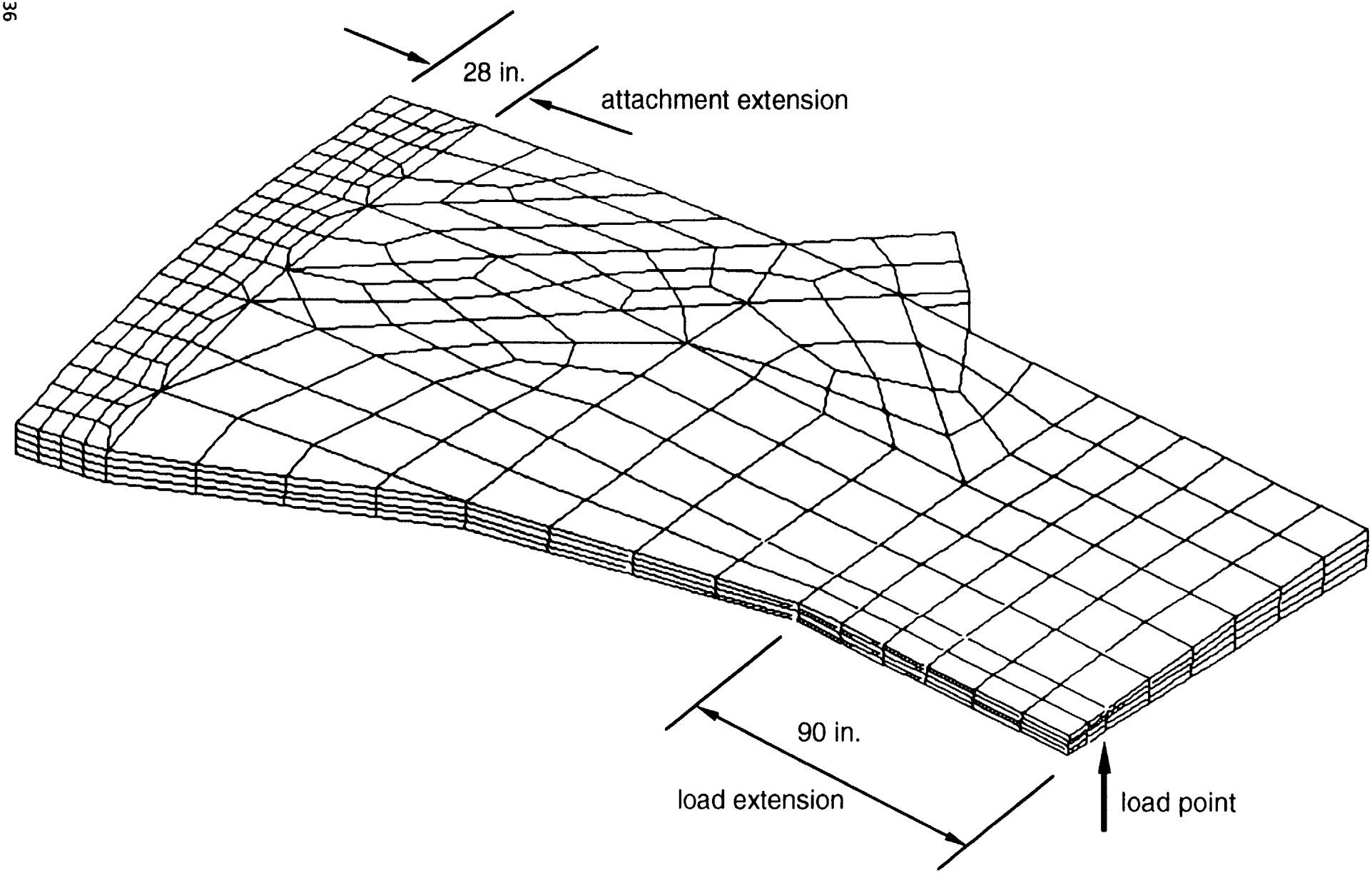

Figure 10.- Proposed HSR wing box structure with test attachments

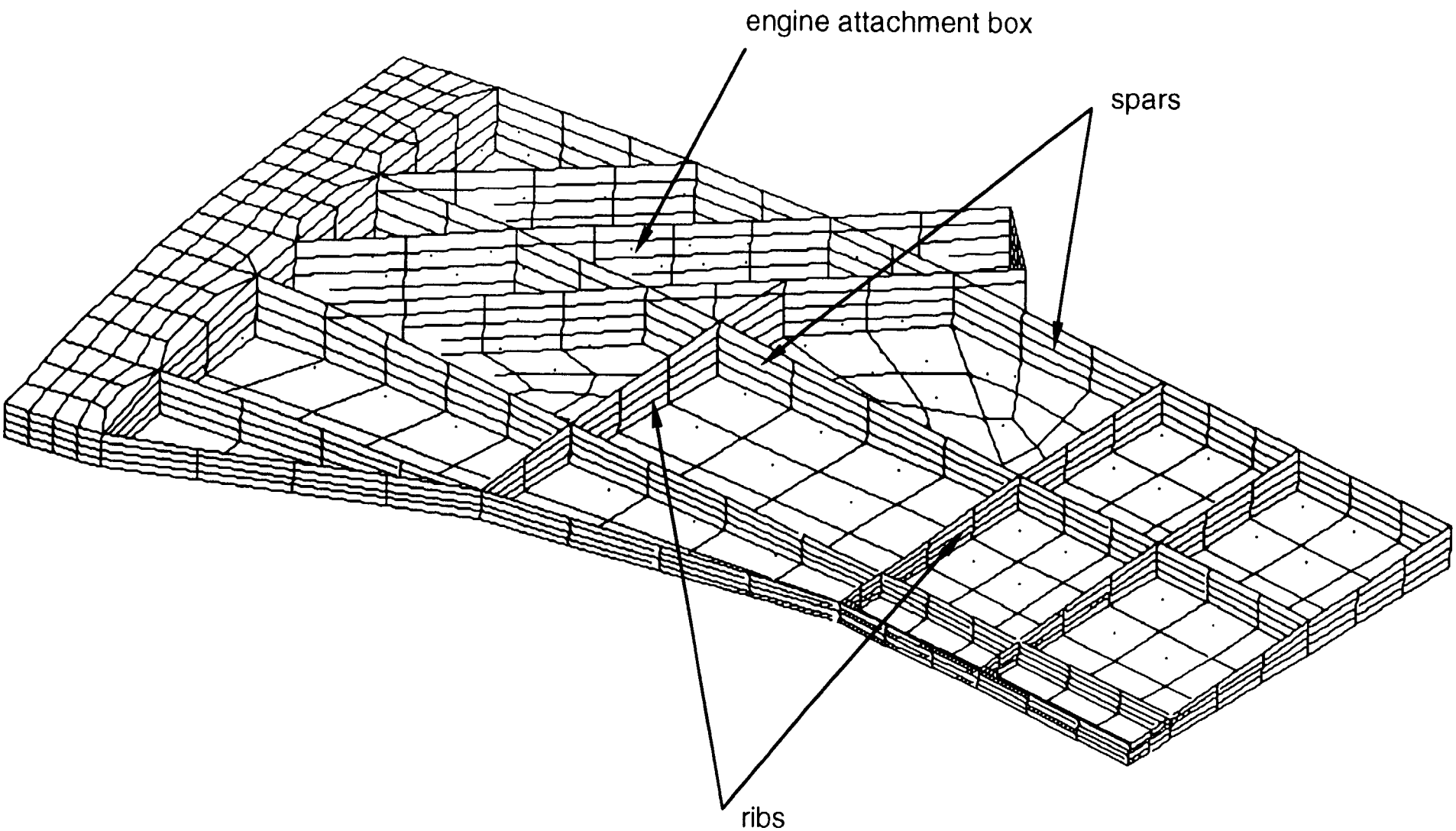

Figure 11.- Proposed HSR wing box - internal structure

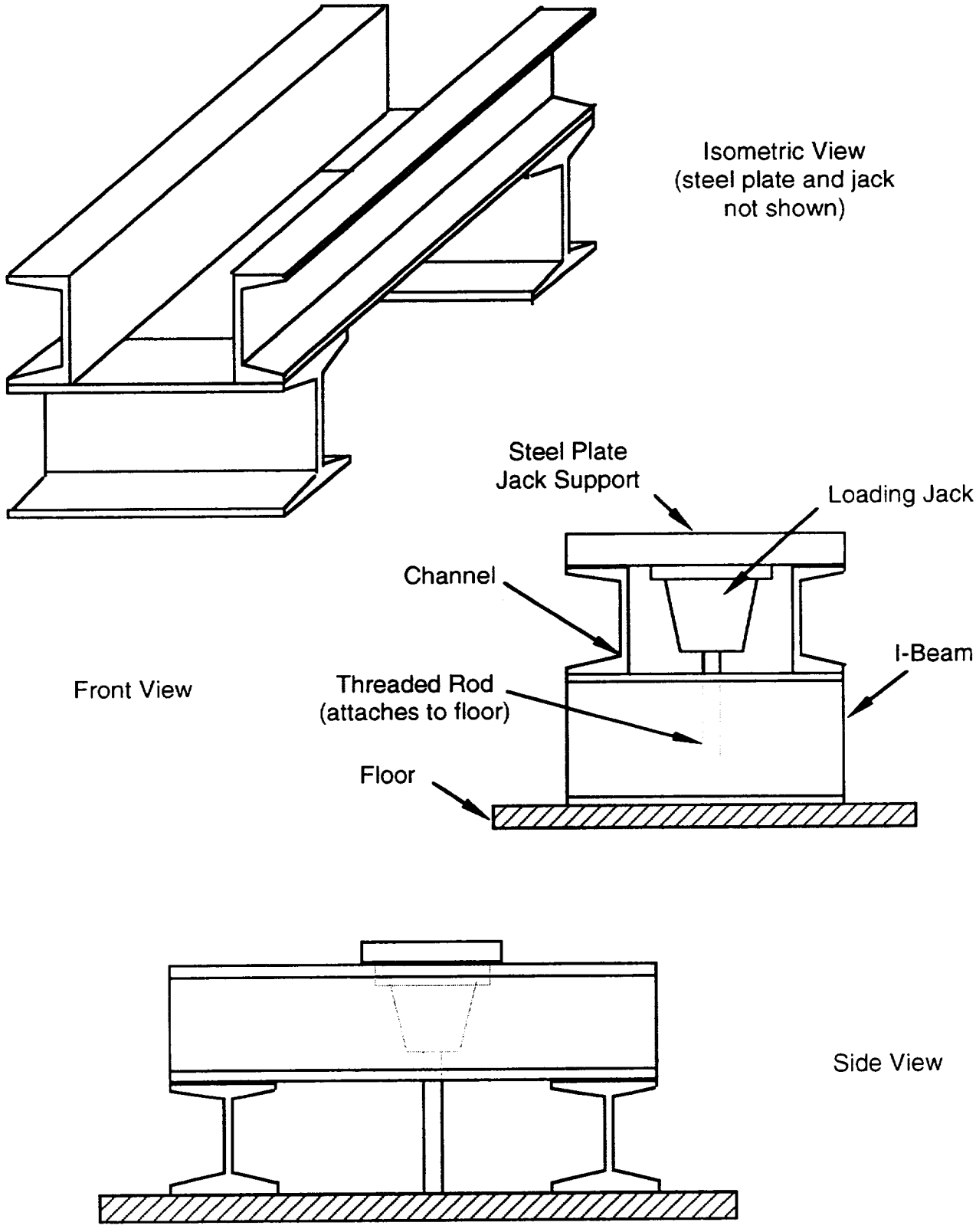

Figure 12.- Floor load test rig

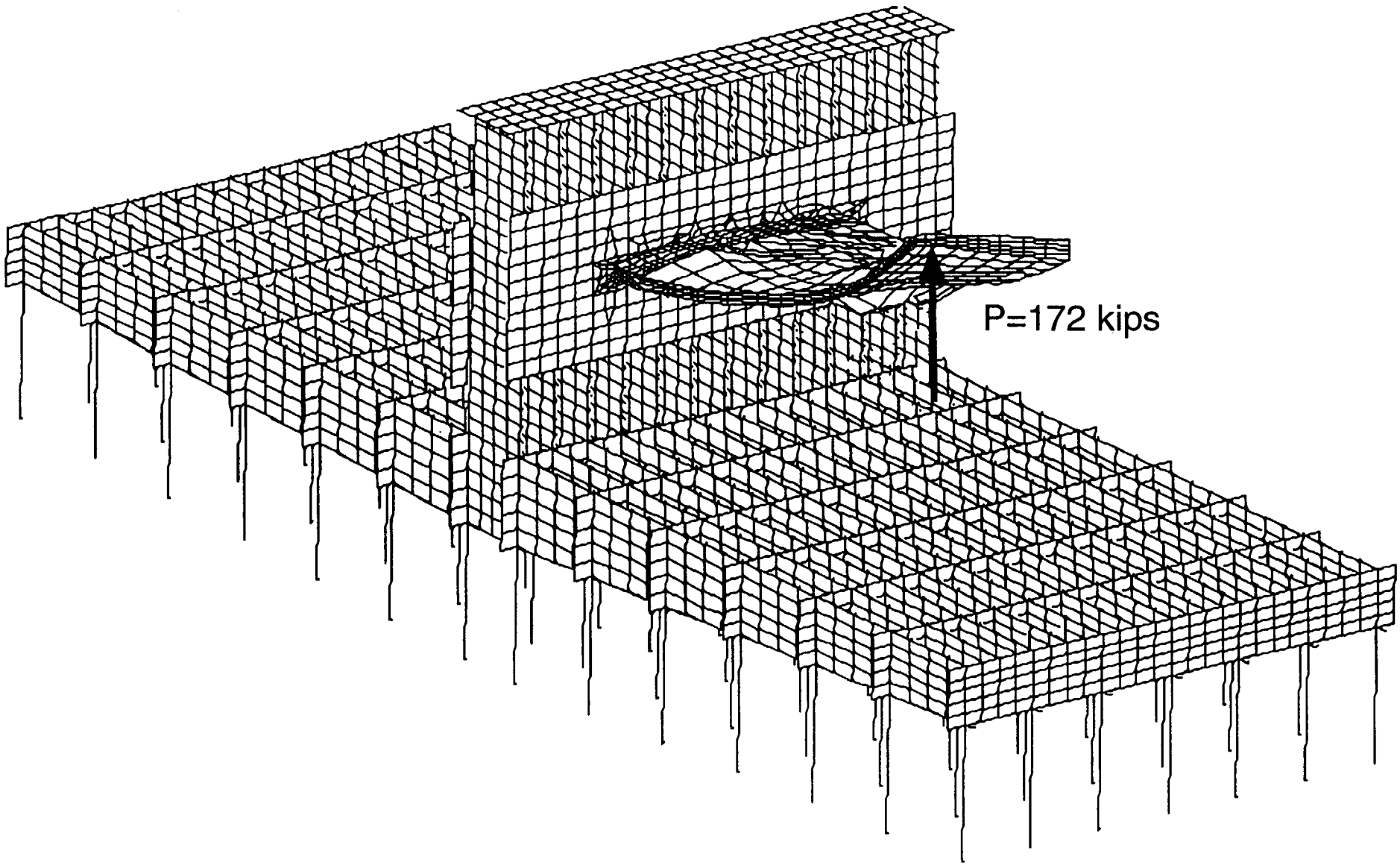

Figure 13.- Deformed shape for HSR wing box attached to backstop

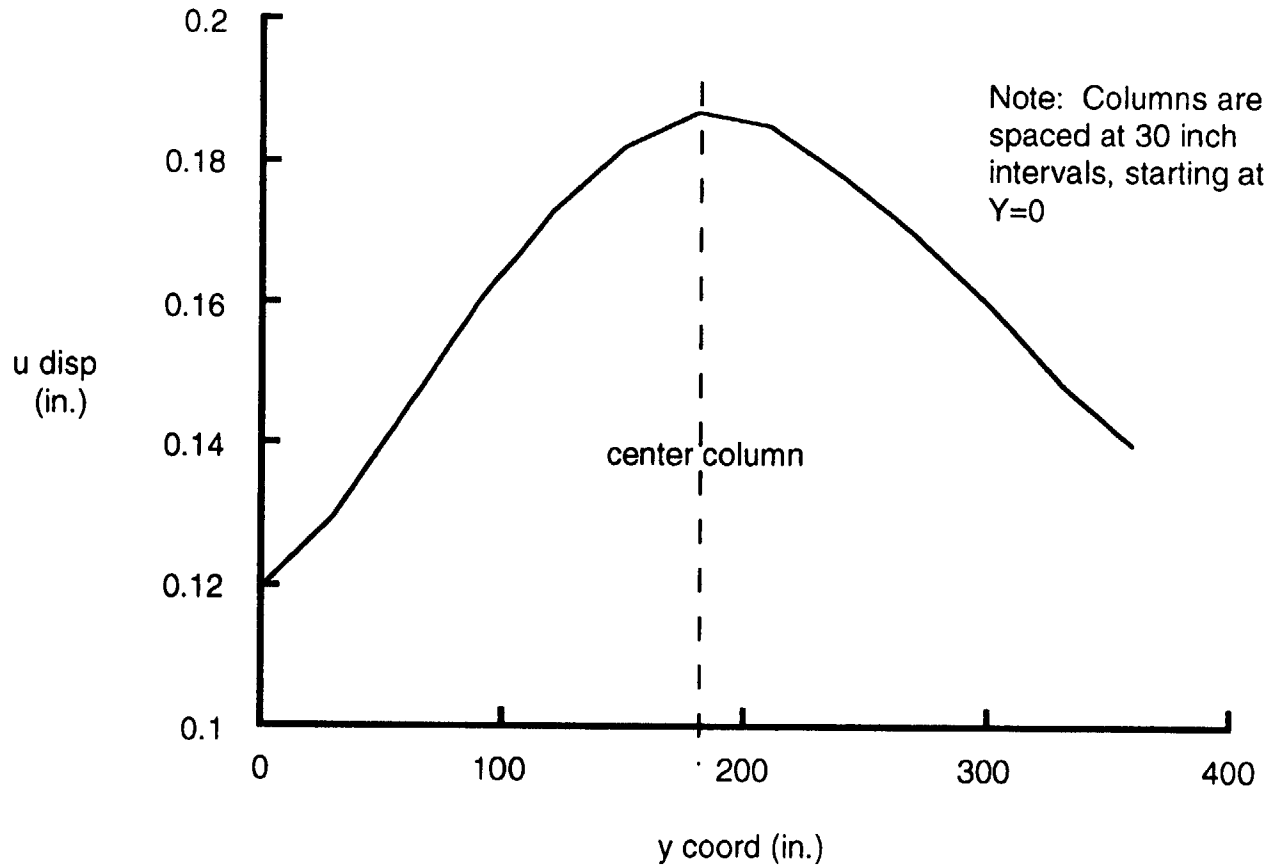

Figure 14.- Displacement at column tops along backstop, HSR wing box with 172 kip tip load

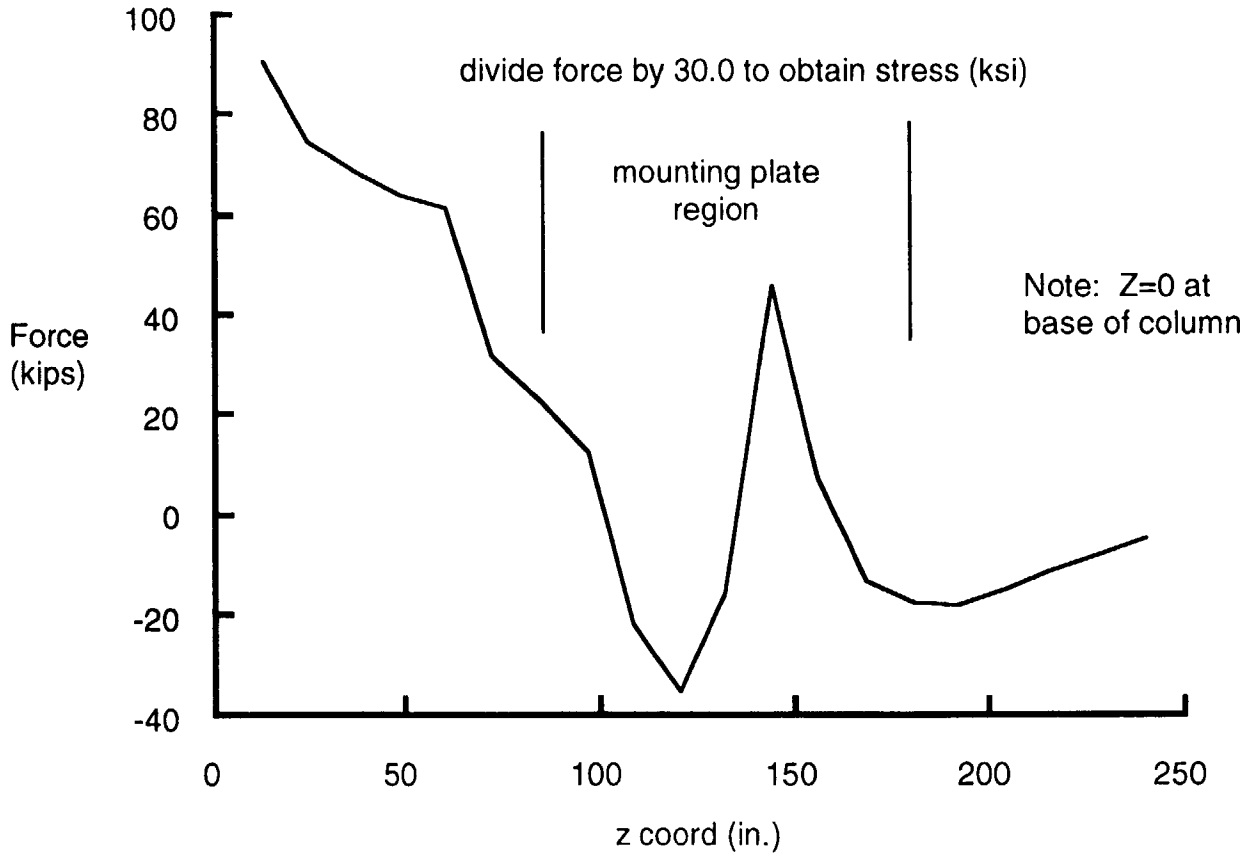

Figure 15.- Force in front flange of middle column, HSR wing box with 172 kip load

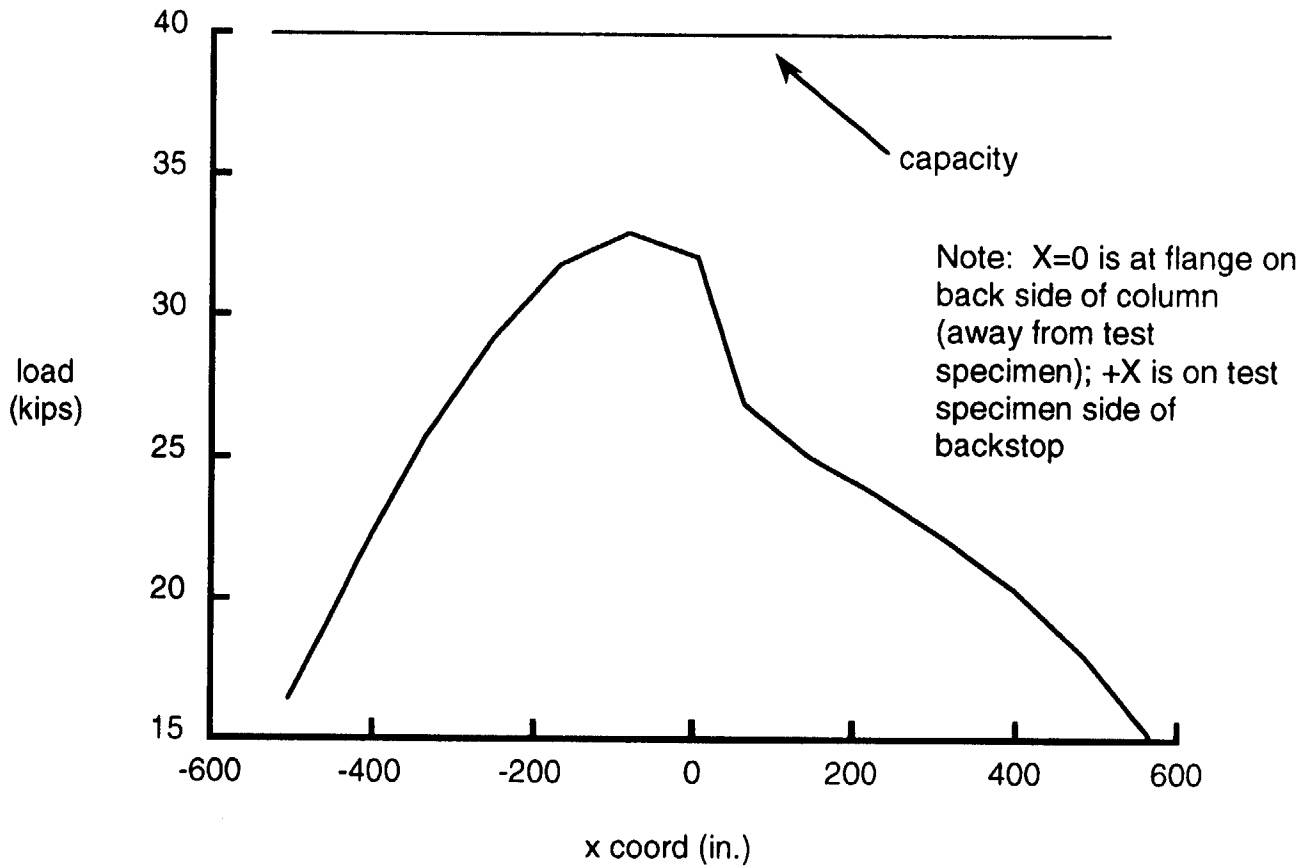

Figure 16.- Pile loads for middle floor beam, HSR wing box with 172 kip tip load

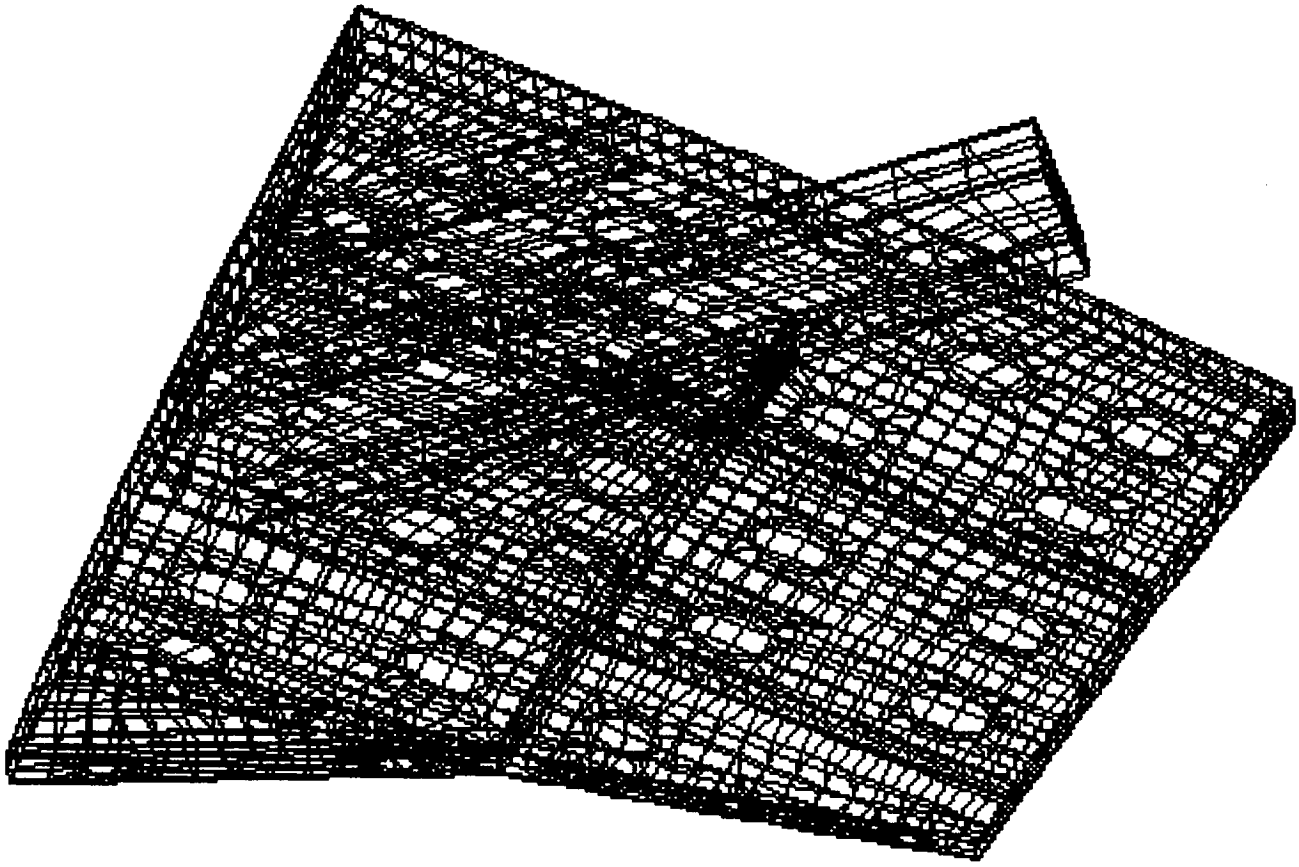

Figure 17.– Finite element model as received

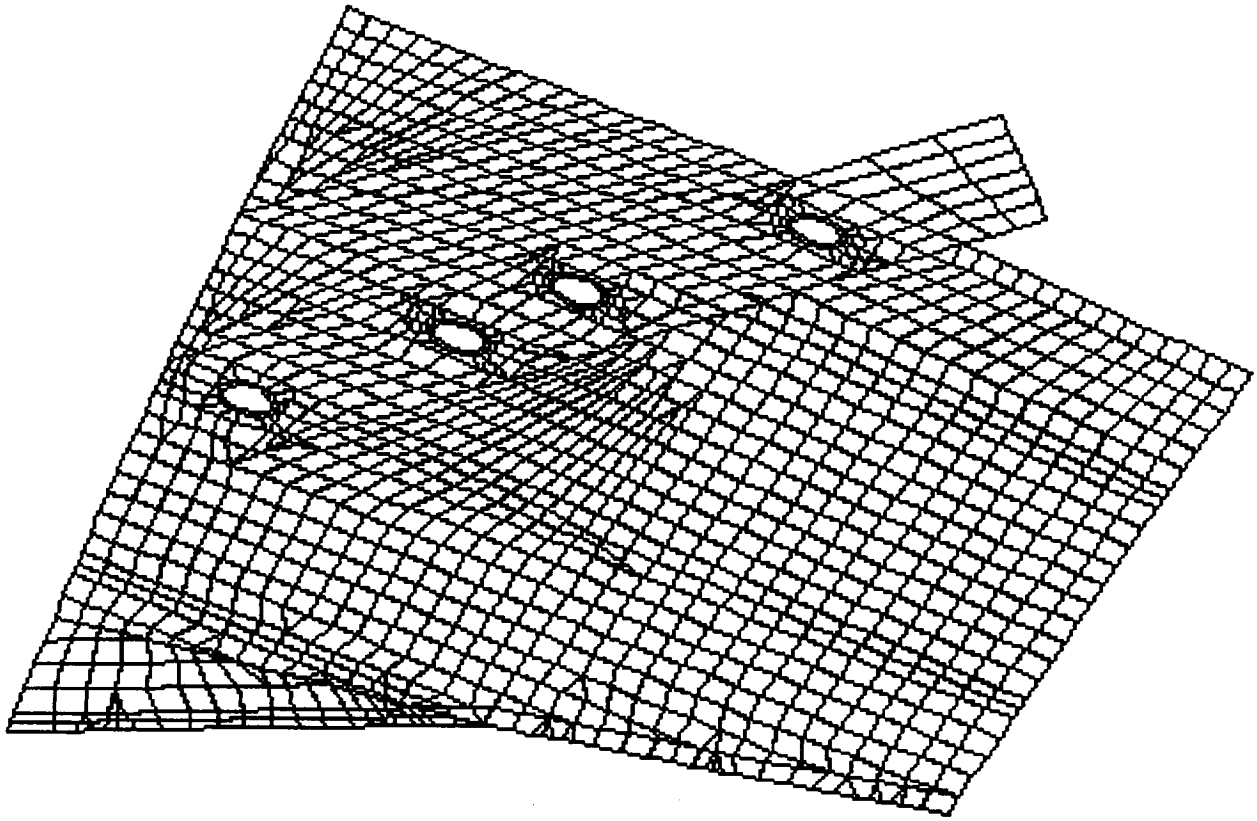

Figure 18.– Upper surface elements

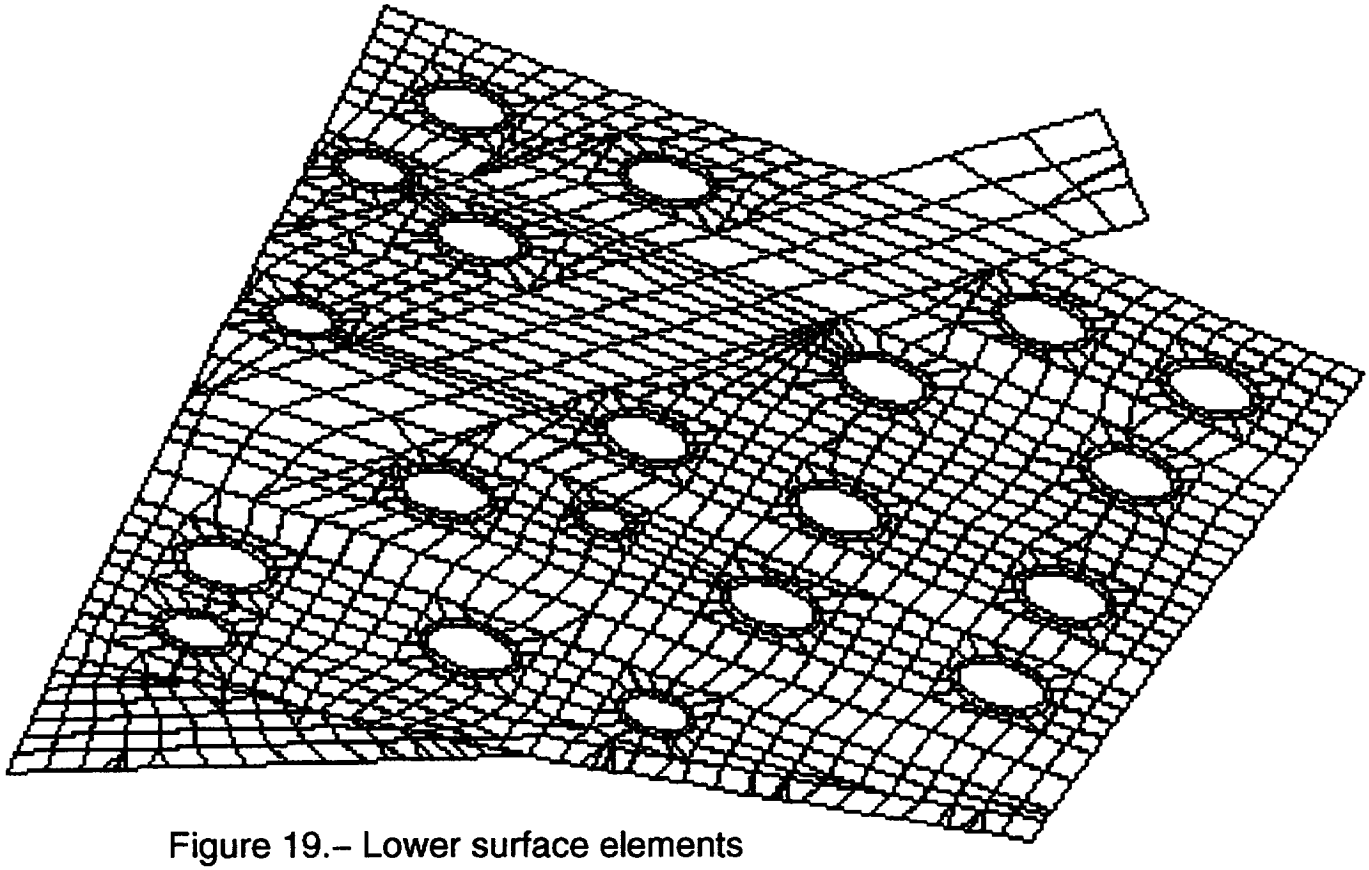

Figure 19.– Lower surface elements

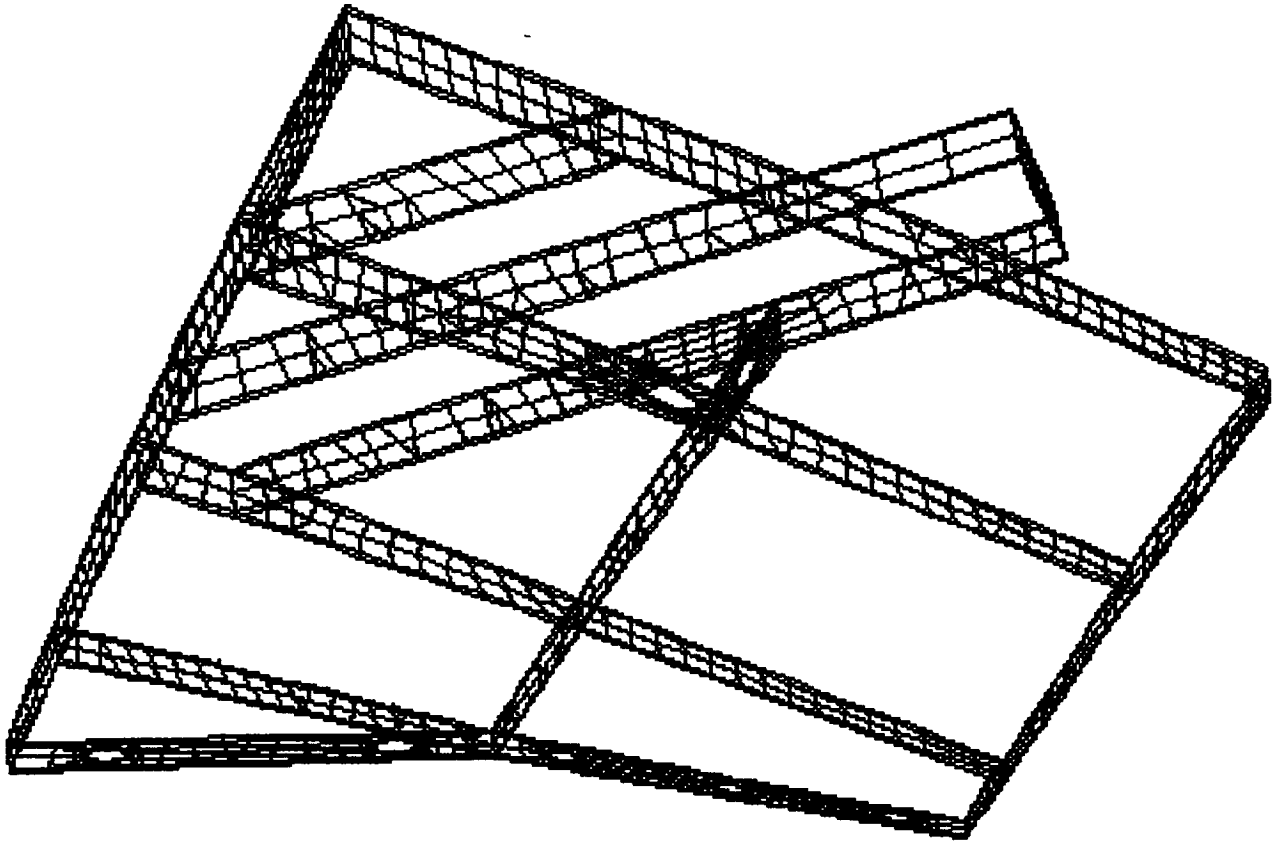

Figure 20.– Internal structure, webs

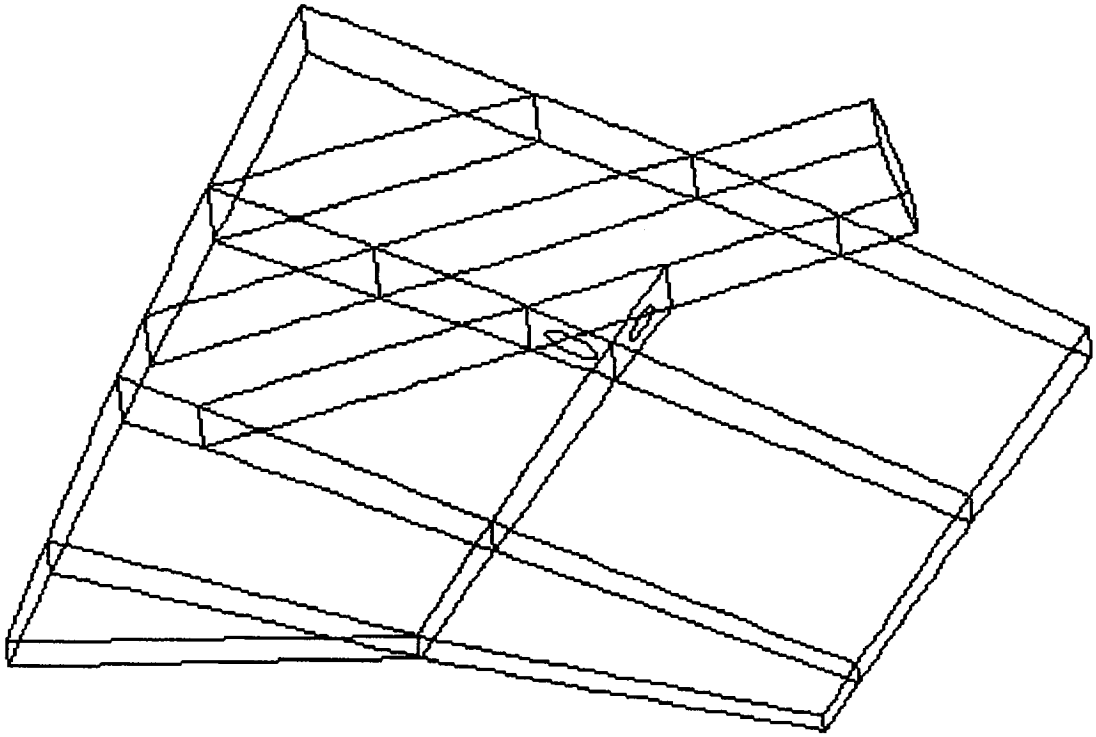

Figure 21.– Internal structure, bars

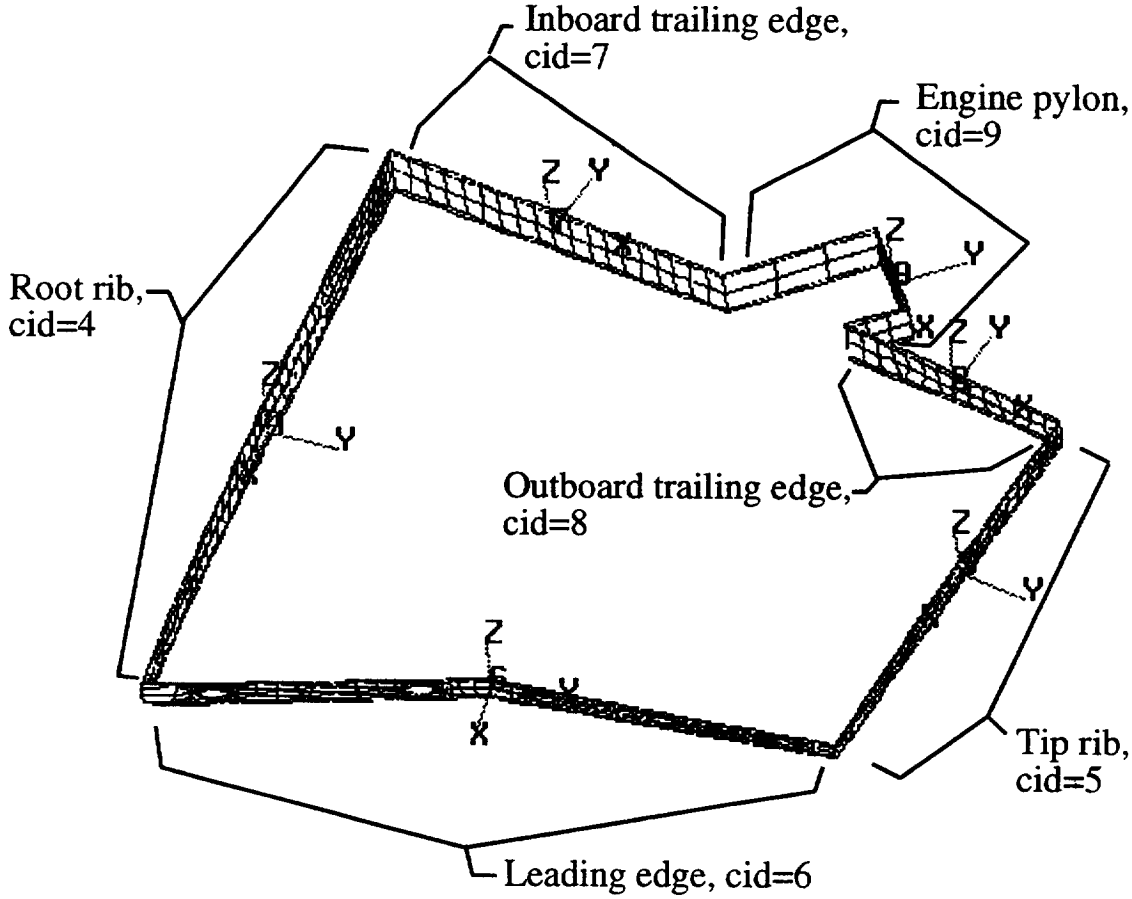

Figure 22.– Locations for force summation of applied mechanical loads

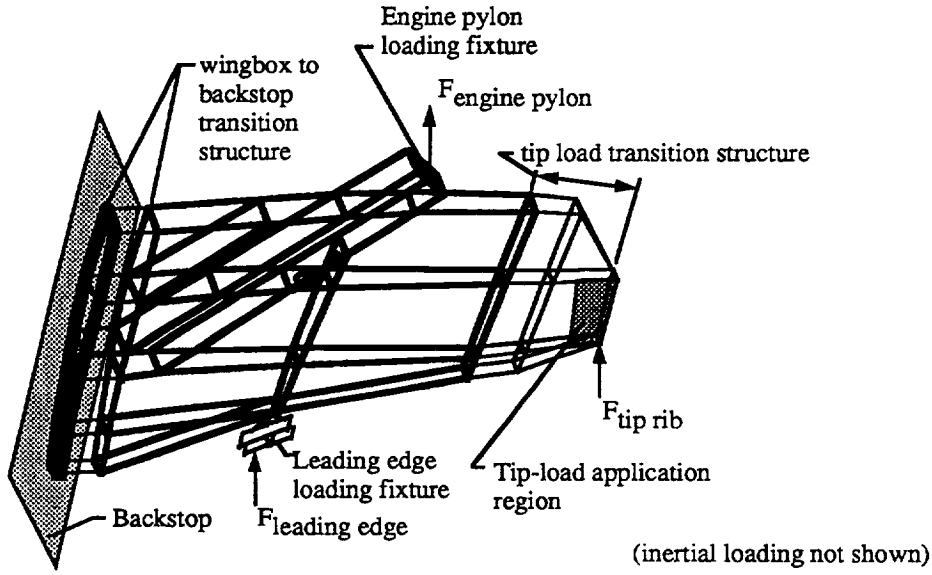

Figure 23.- Actuator arrangement 1,
single actuator used to supply tip load

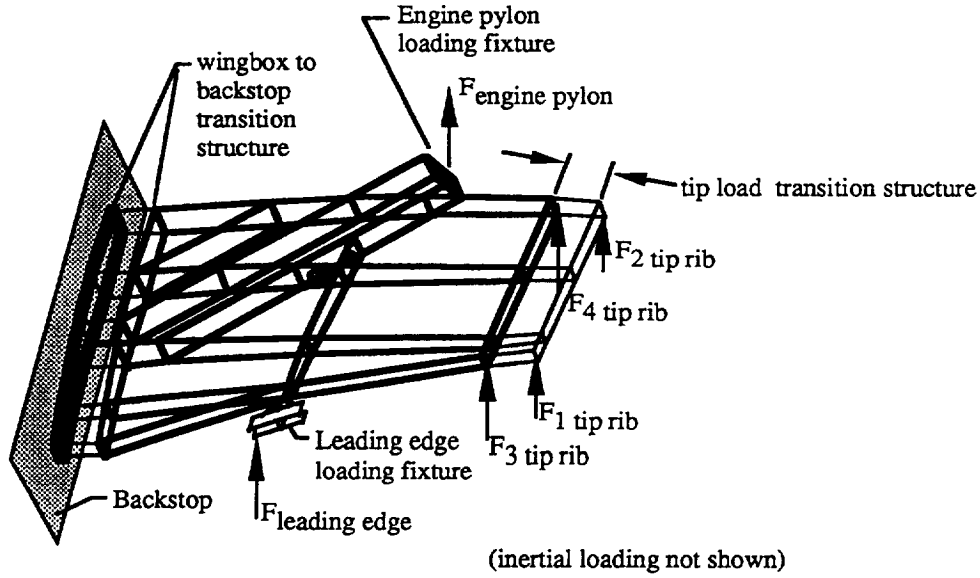

Figure 24.- Actuator arrangement 2,
multiple actuators used to supply tip load

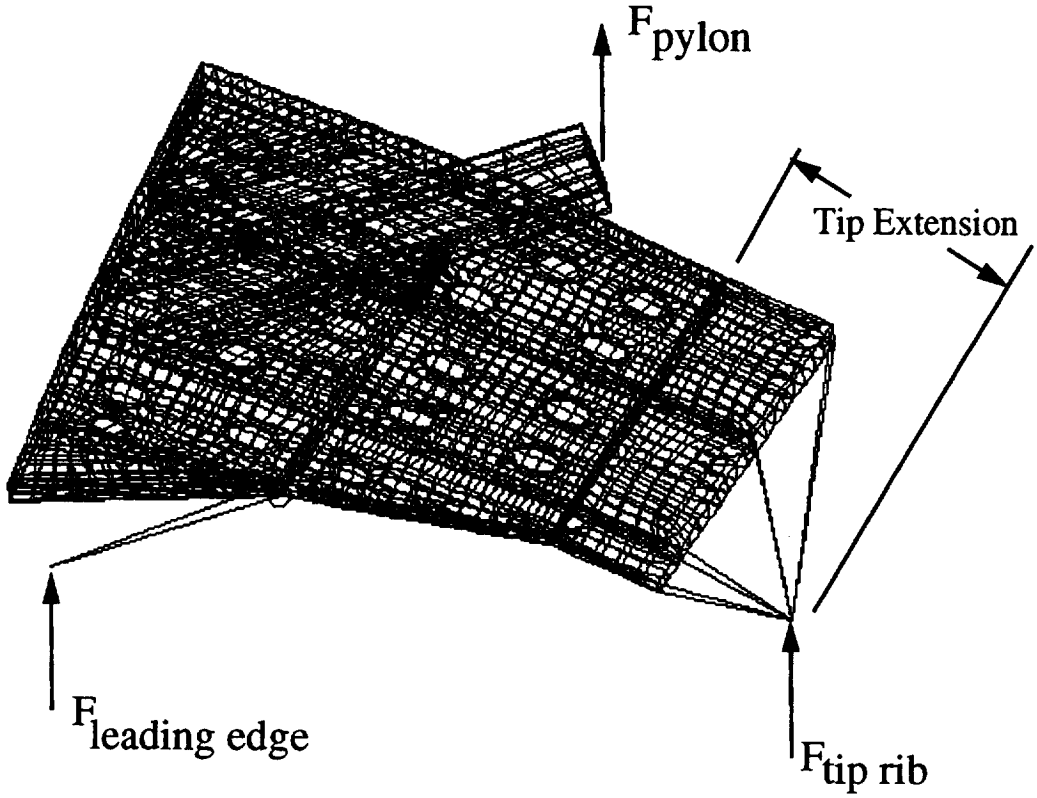

Figure 25.– Finite element model with tip extension as required for actuator arrangement 1, single actuator at tip rib

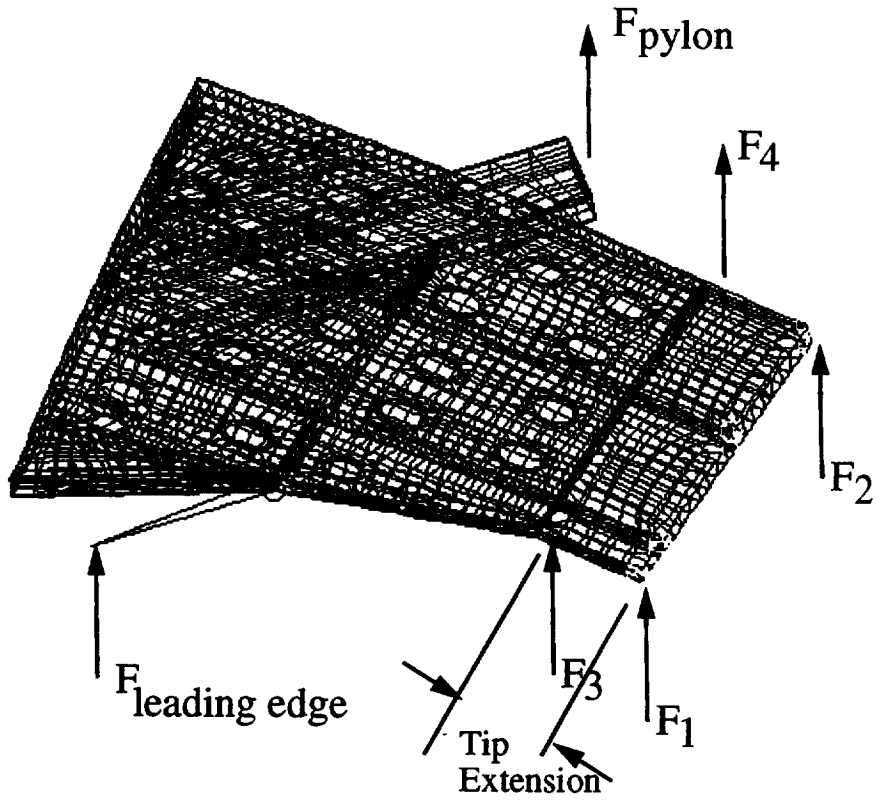

Figure 26.– Finite element model with tip extension as required for actuator arrangement 2, multiple actuators at tip rib

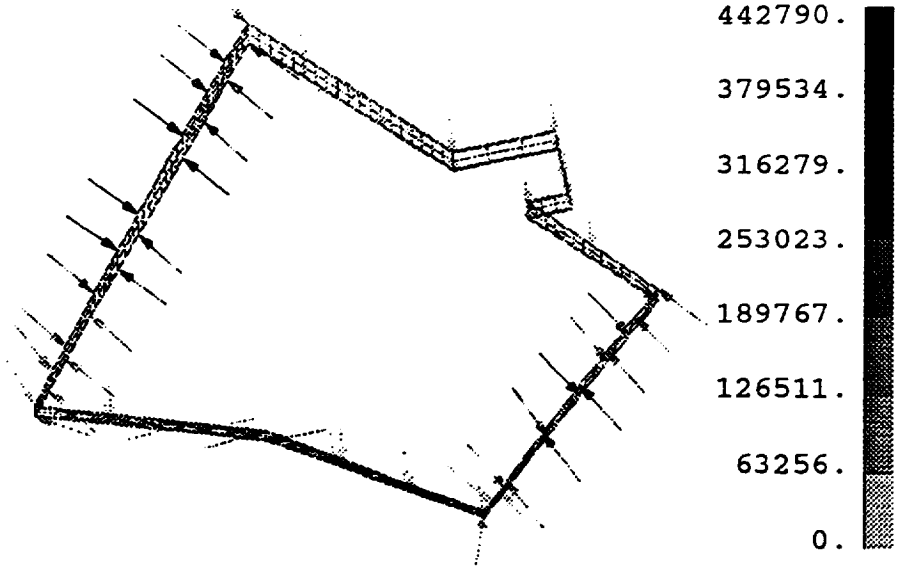

Figure 27.– MDAC translational applied loads on the wingbox boundary

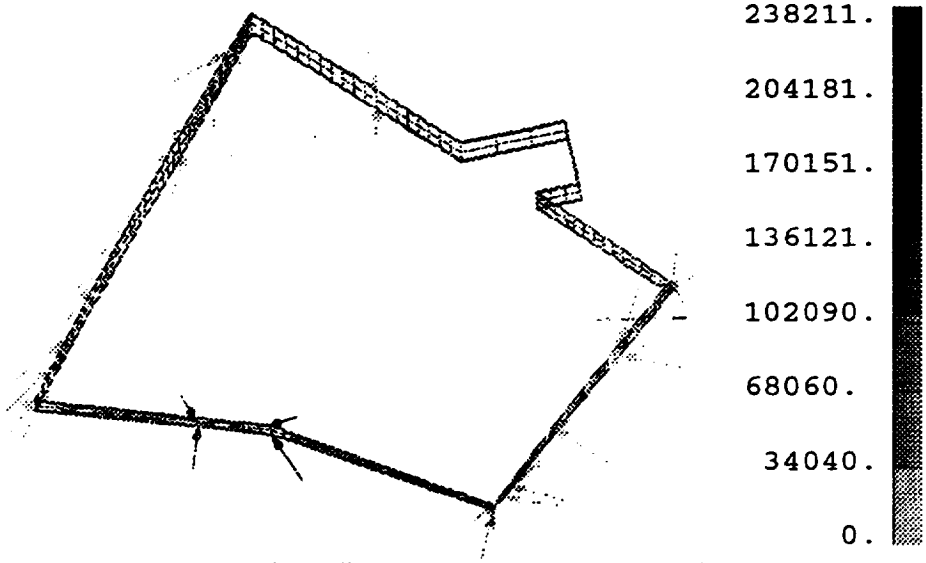

Figure 28.– MDA rotational applied loads on the wingbox boundary

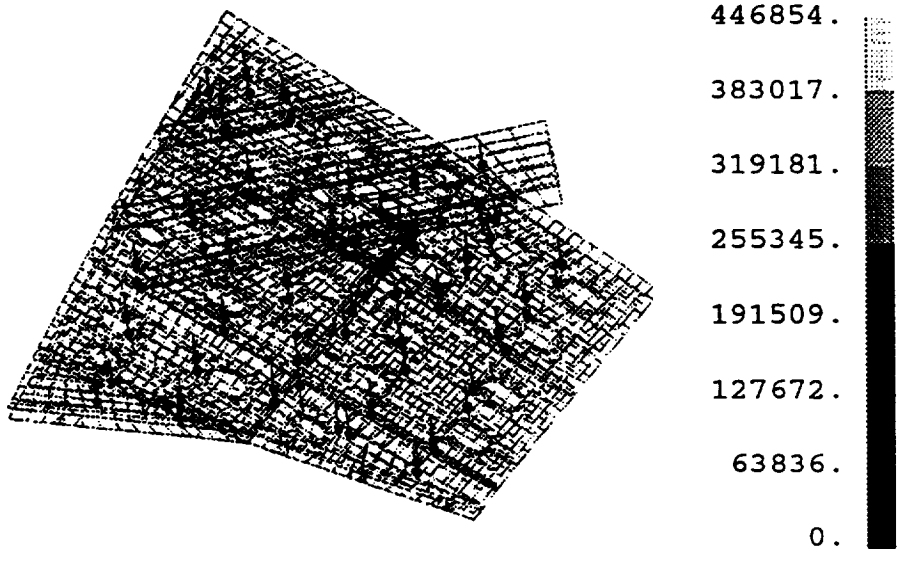

Figure 29.– MDAC translational applied loads on the wingbox internal structure

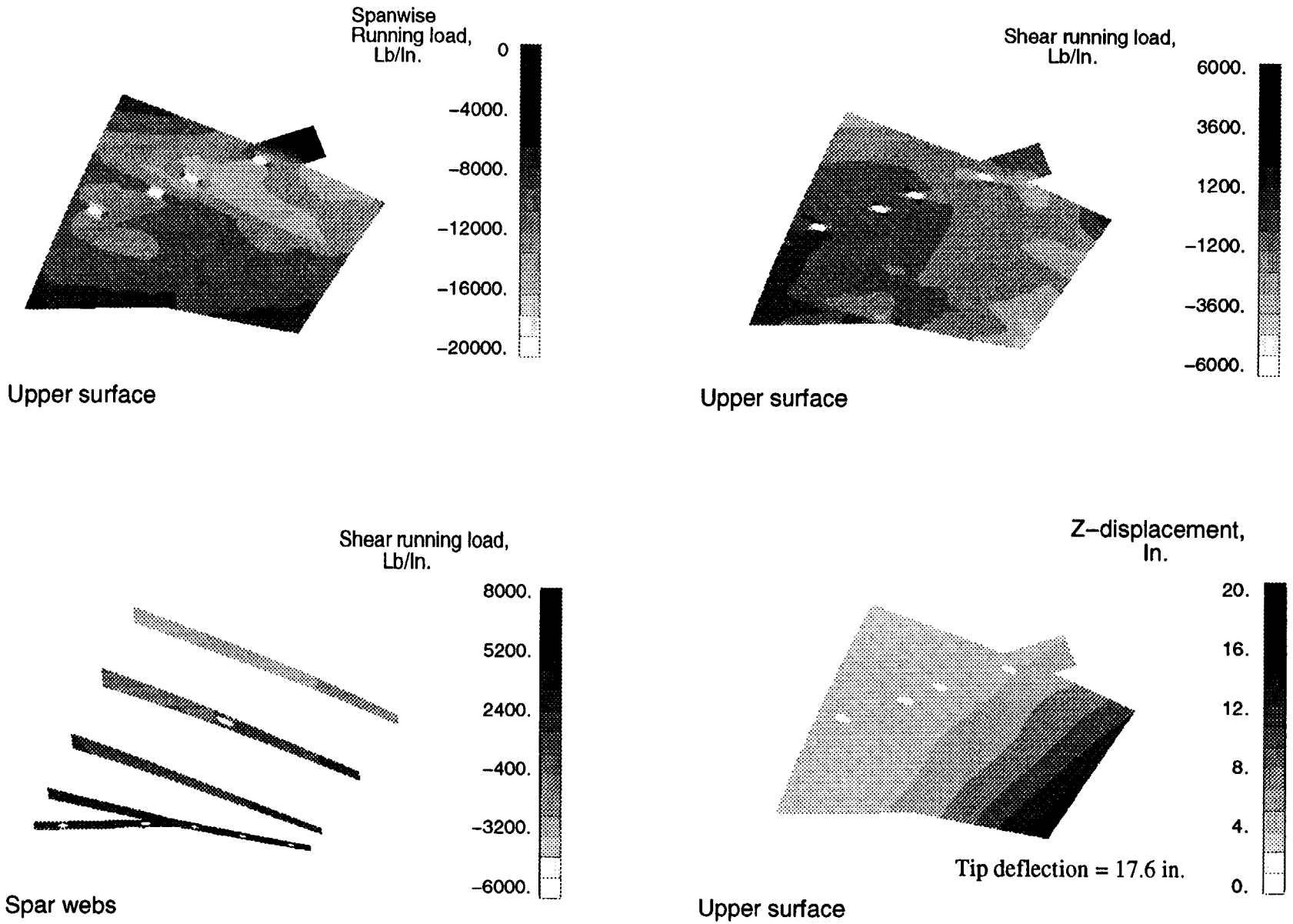

Figure 30.– Forces in structural elements for the 3.75g mach .95 pullup condition, MDAC applied flight loads

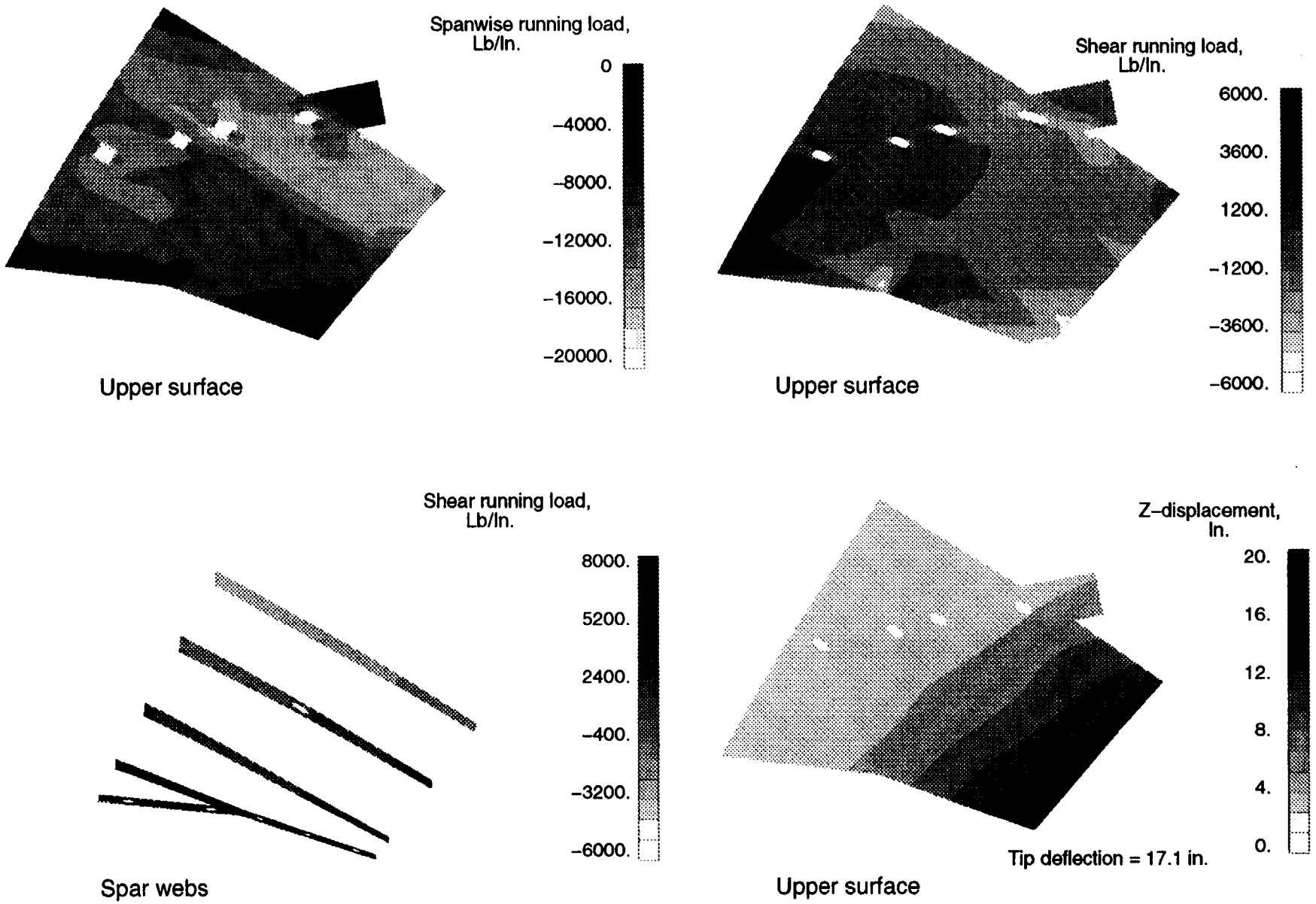

Figure 31.– Forces in structural elements for the 3.75G mach .95 pullup condition, actuator induced mechanical loading

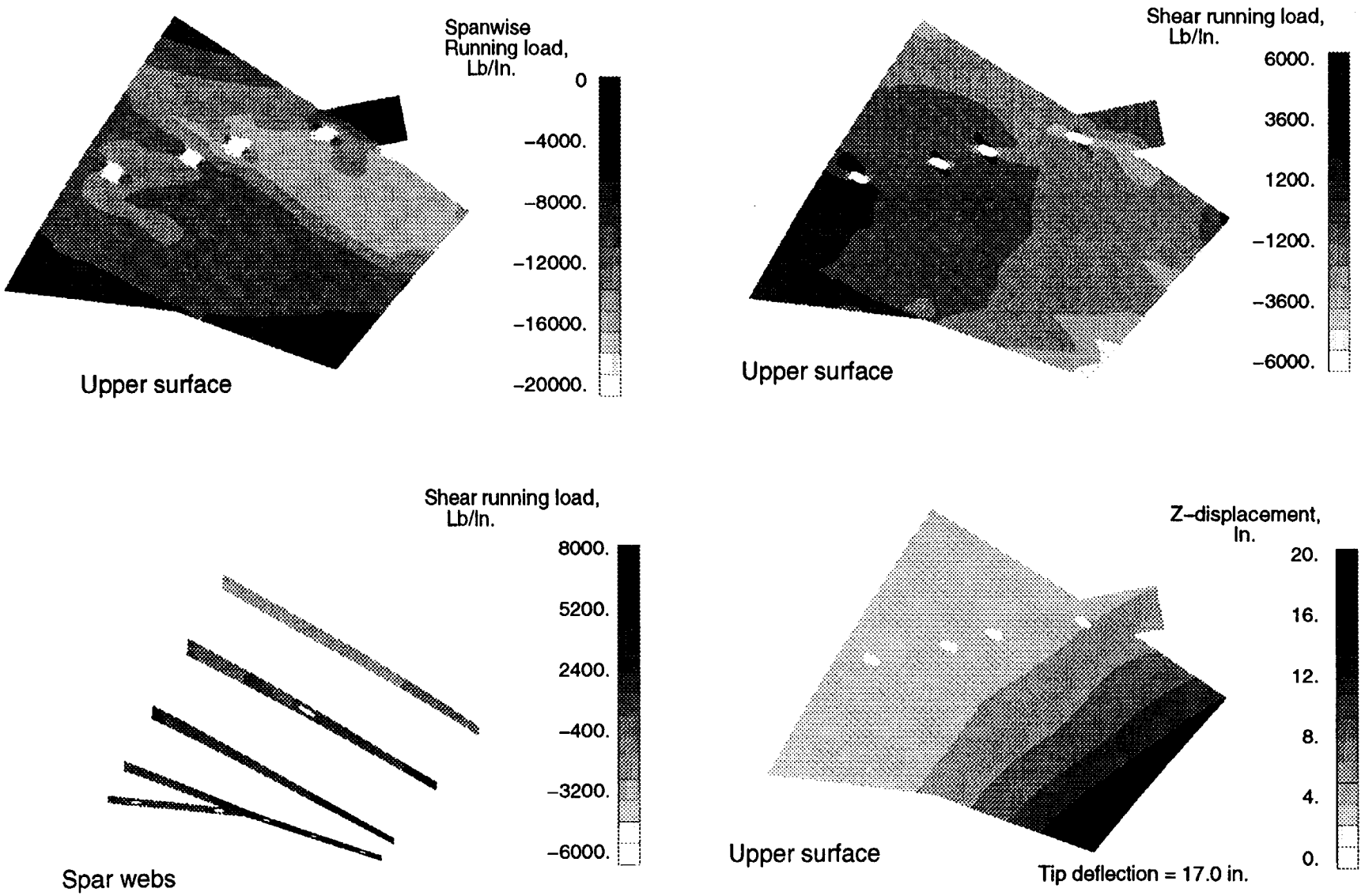

Figure 32.– Forces in Structural Elements for the 3.75g mach .95 pullup condition, actuator induced mechanical loads, no leading edge load

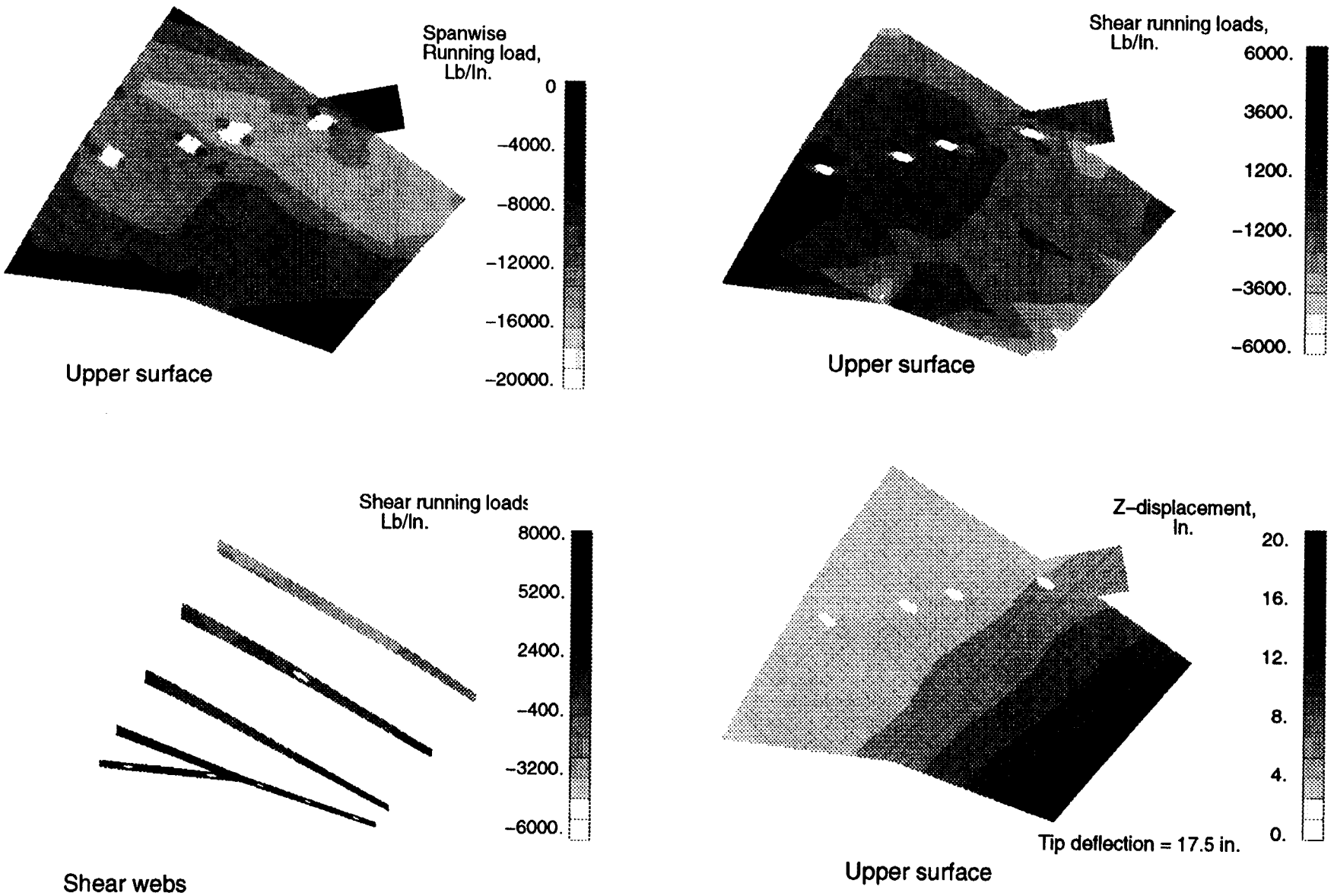

Figure 33.– Forces in structural elements for the 3.75g mach .95 pullup condition, actuator induced mechanical loads, no engine pylon load

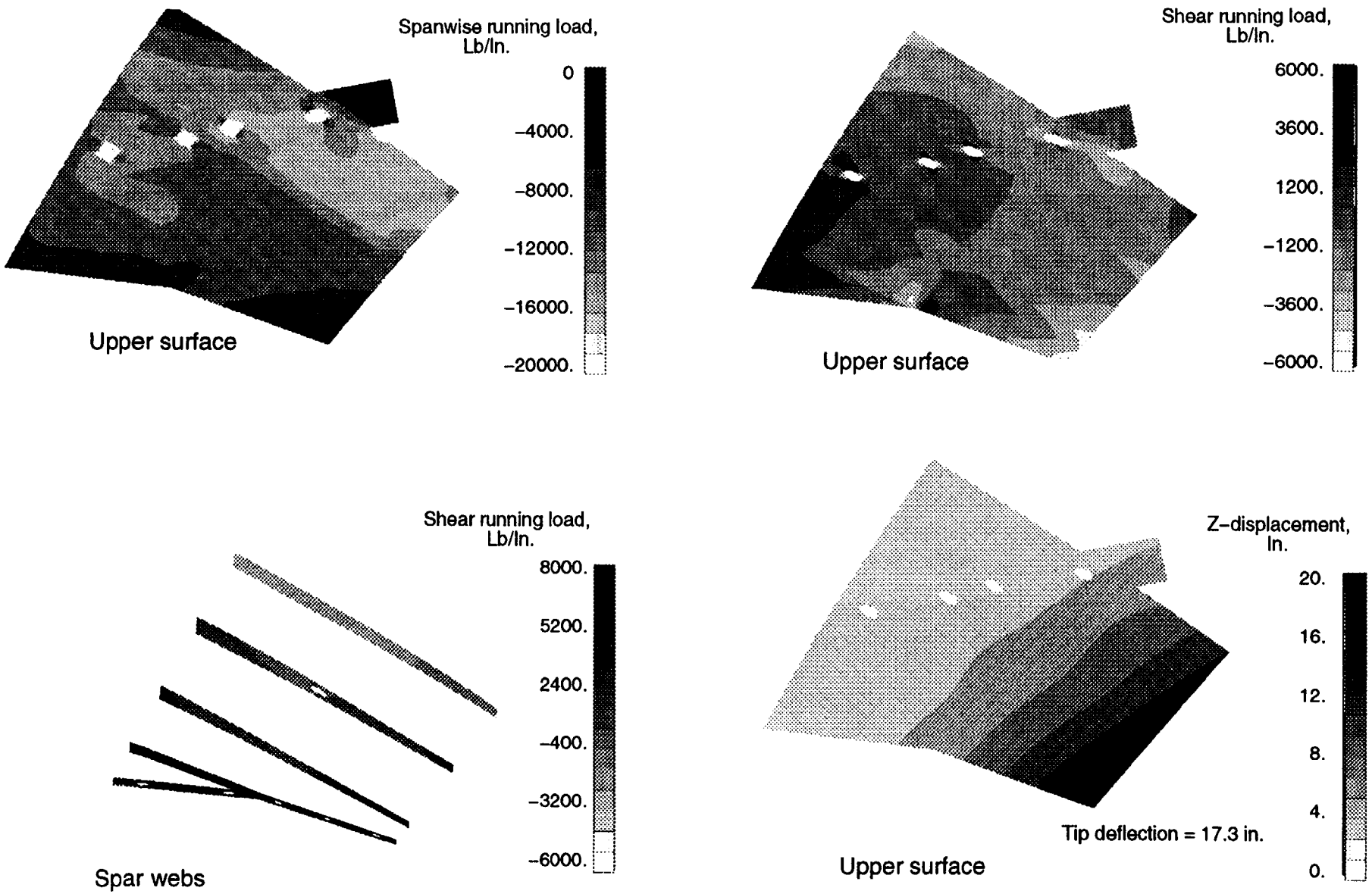

Figure 34.– Forces in structural elements fpr the 3.75g mach .95 pullup condition, actuator induced mechanical loads, no inertial loads

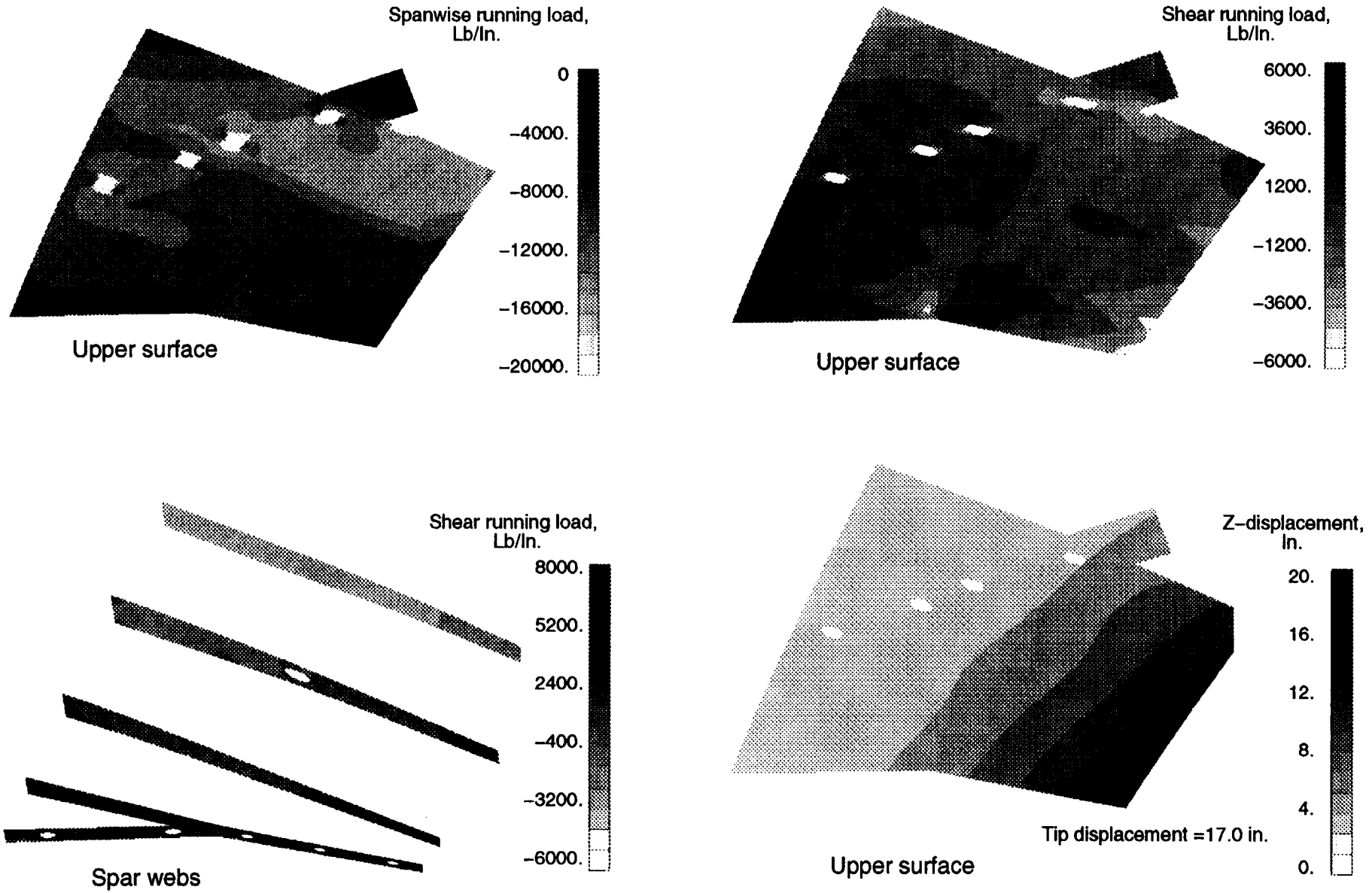

Figure 35.– Forces in structural elements for the 3.75g mach .95 pullup condition, actuator configuration 2, induced mechanical loads

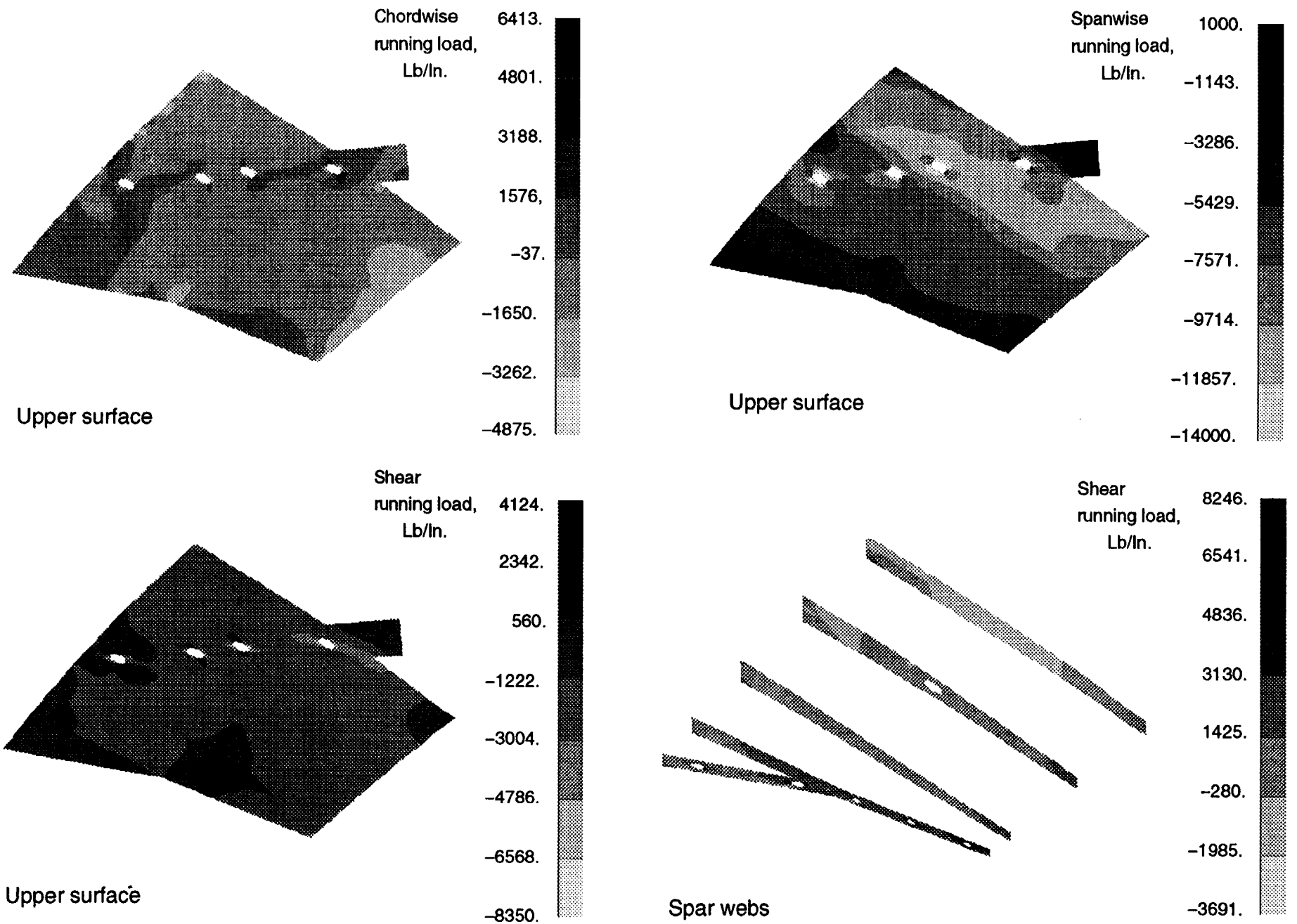

Figure 36.– Forces in structural elements for the 3.75 g mach 2.4 pullup condition, MDAC applied flight loads

Figure 37.– Temperature distribution on upper skin for 3.75G Mach 2.4 flight load case

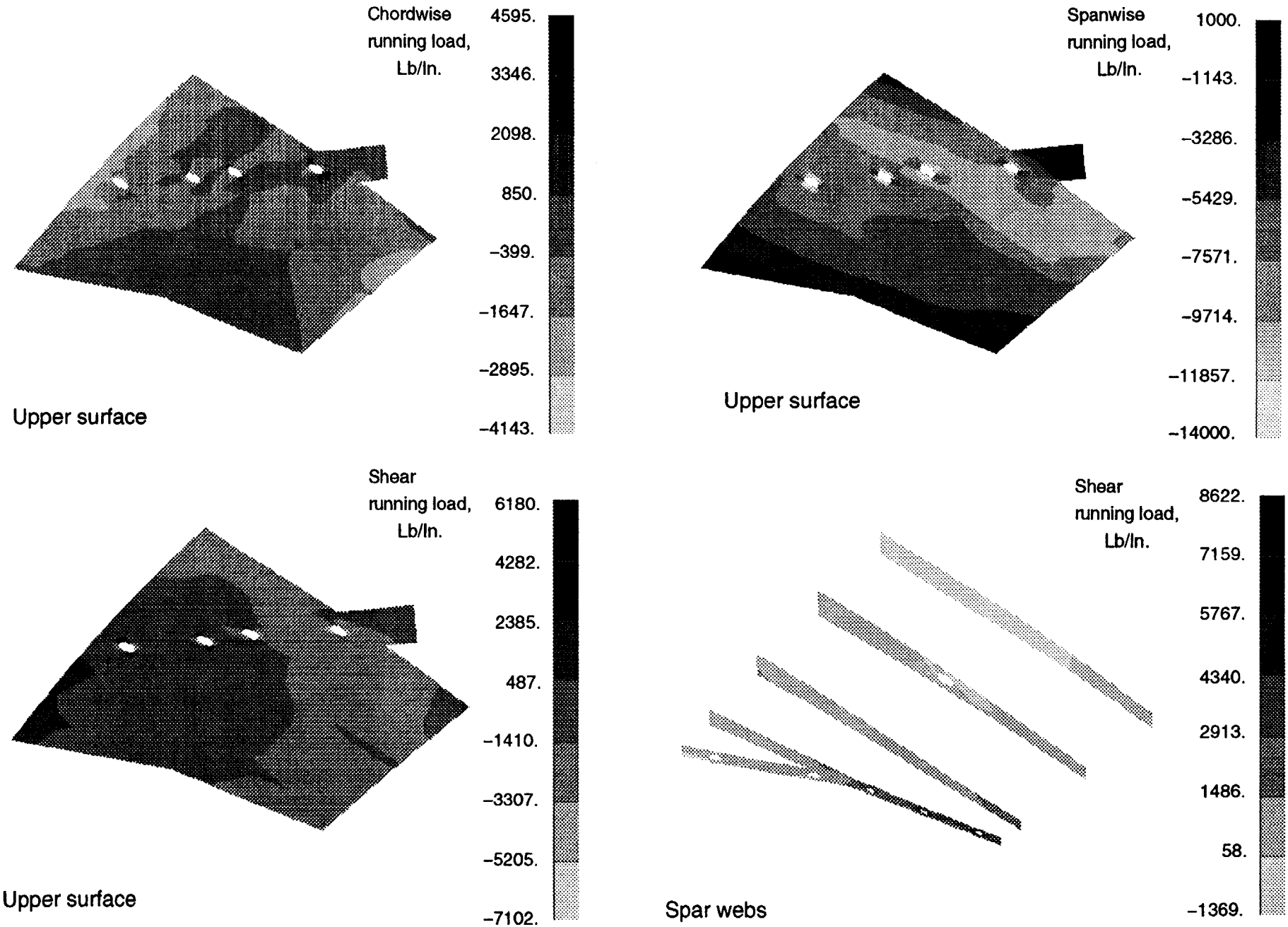

Figure 38.– Forces in structural elements for the 3.75 g mach 2.4 pullup condition, actuator applied mechanical loads only

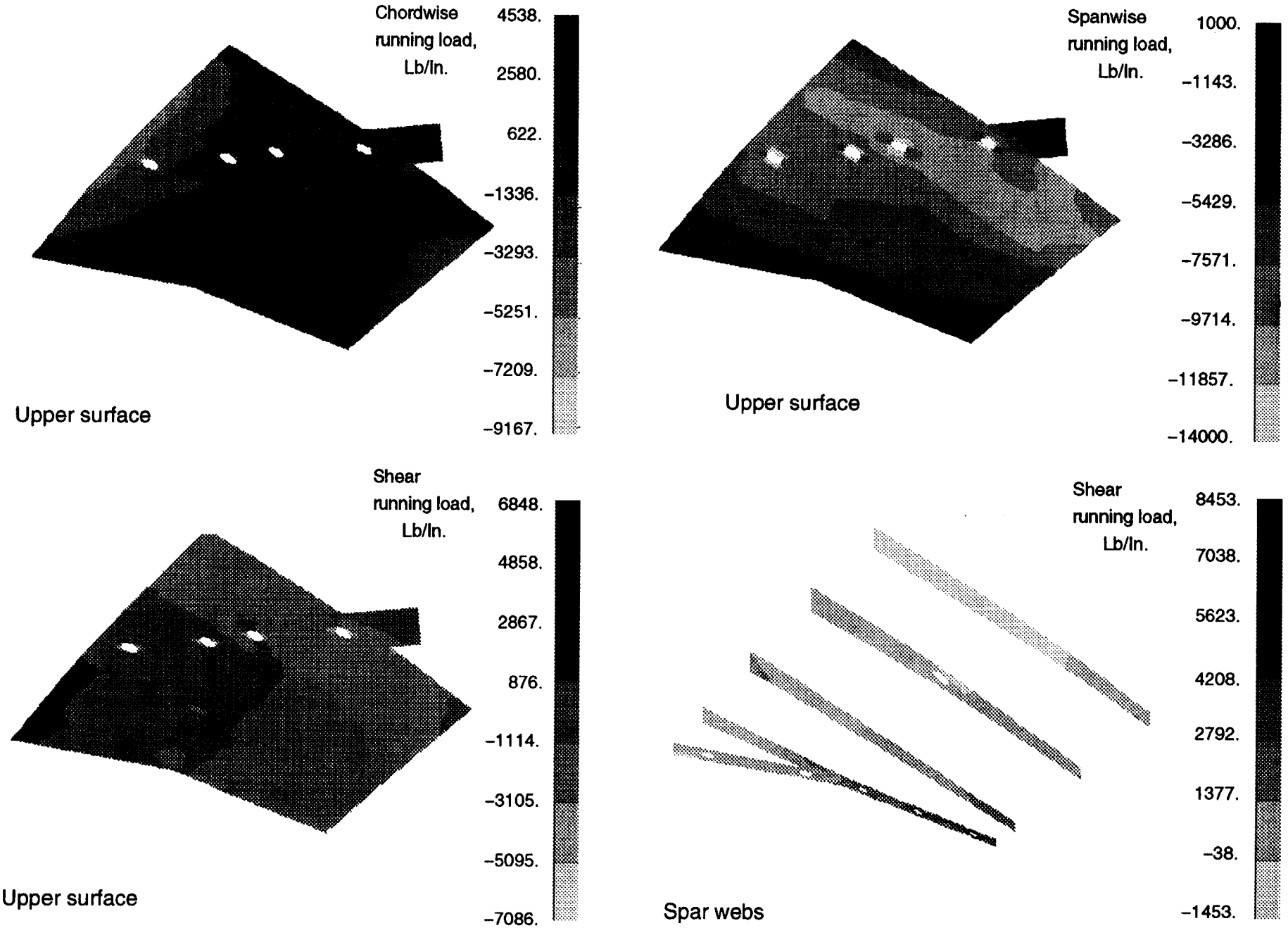

Figure 39.– Forces in structural elements for the 3.75g mach 2.4 pullup condition, actuator applied mechanical loads plus thermal load

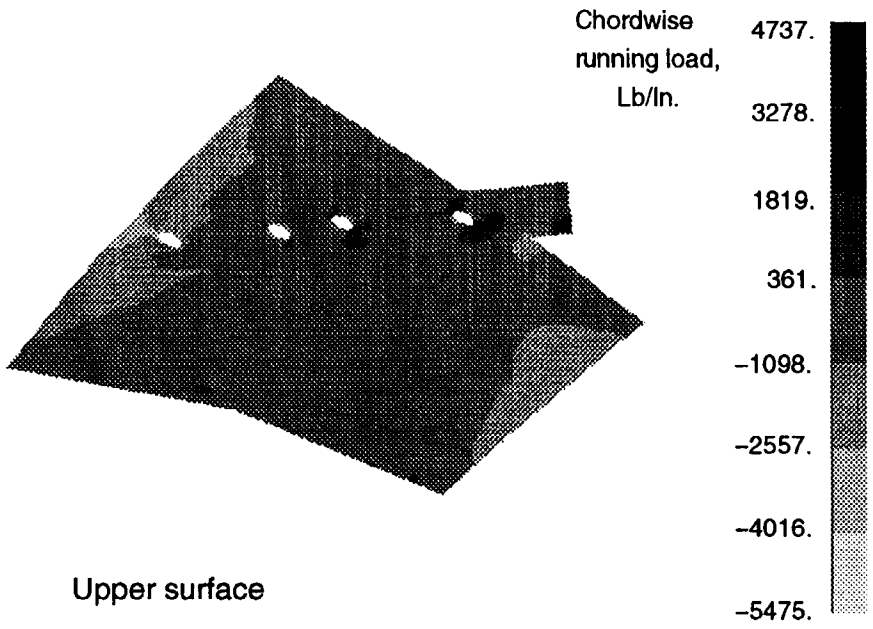

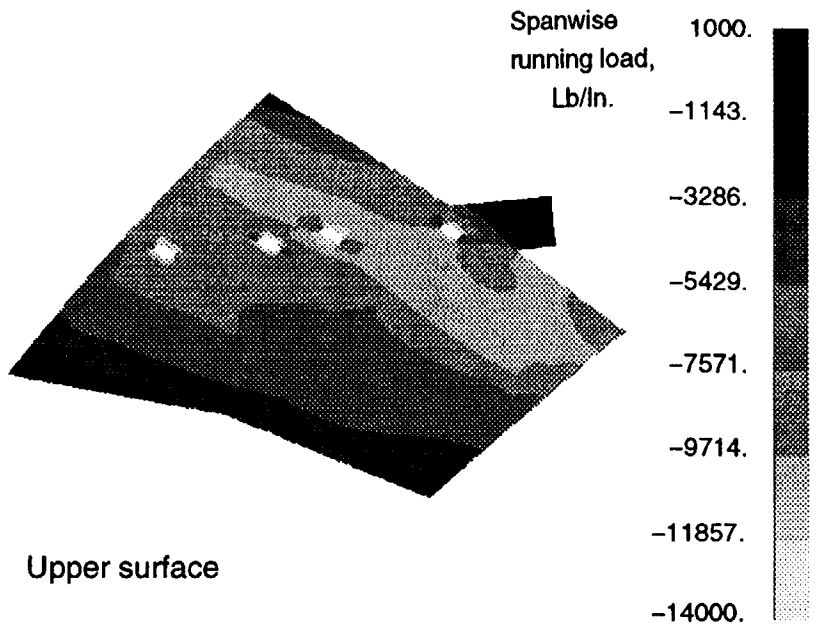

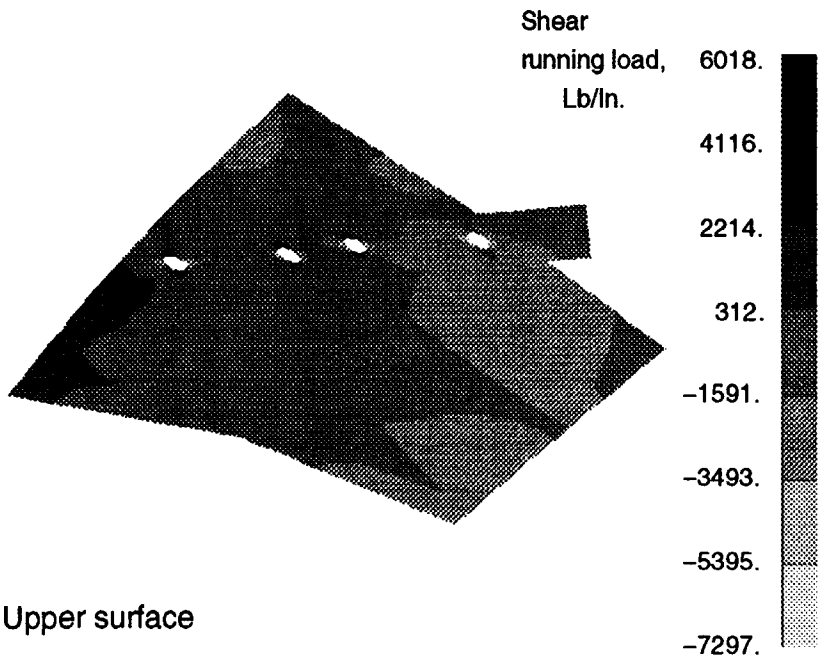

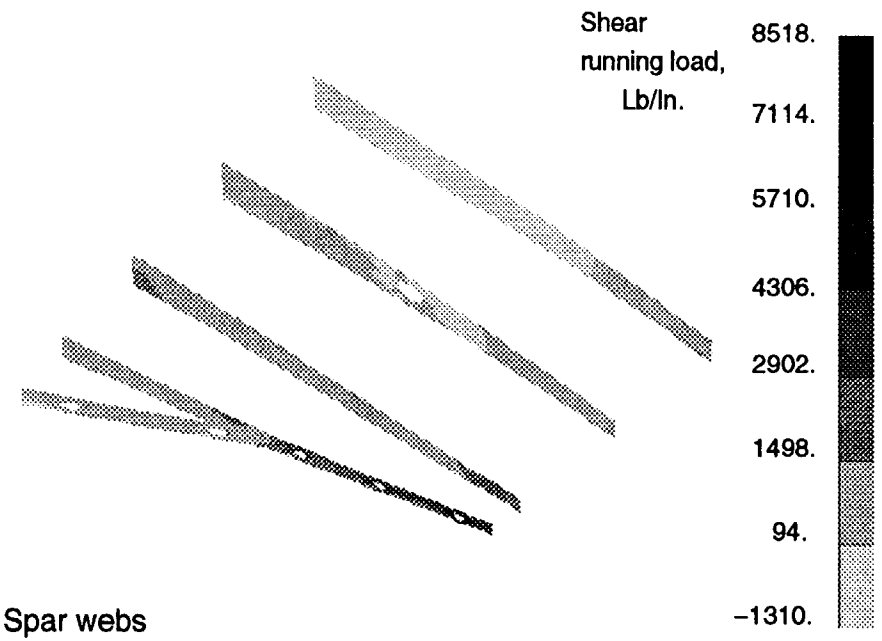

Figure 40.– Forces in structural elements for the 3.75g mach 2.4 pullup condition, actuator applied mechanical loads plus thermal load, titanium structure linking backstop to specimen

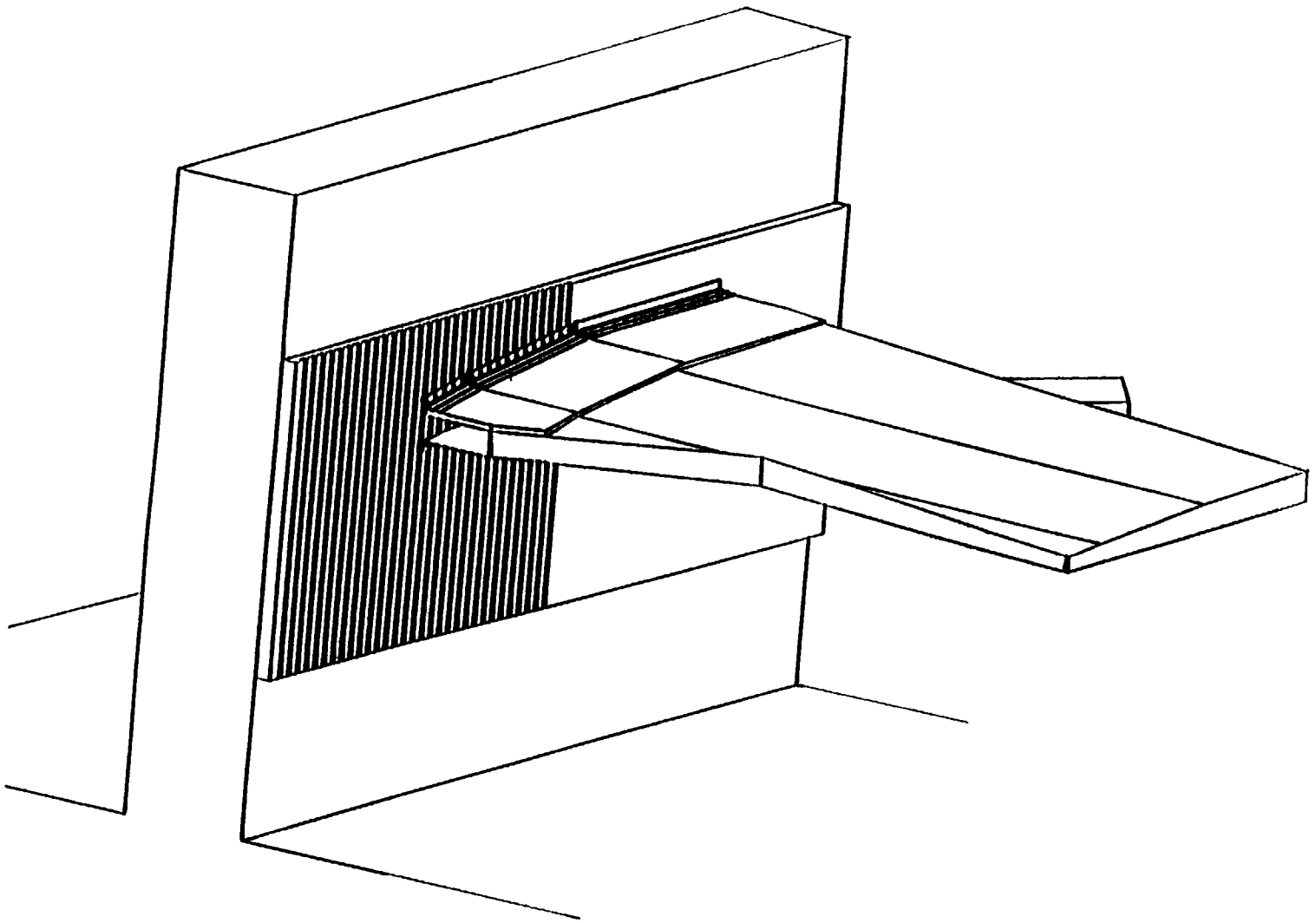

Figure 41.- Wingbox mounted to backstop

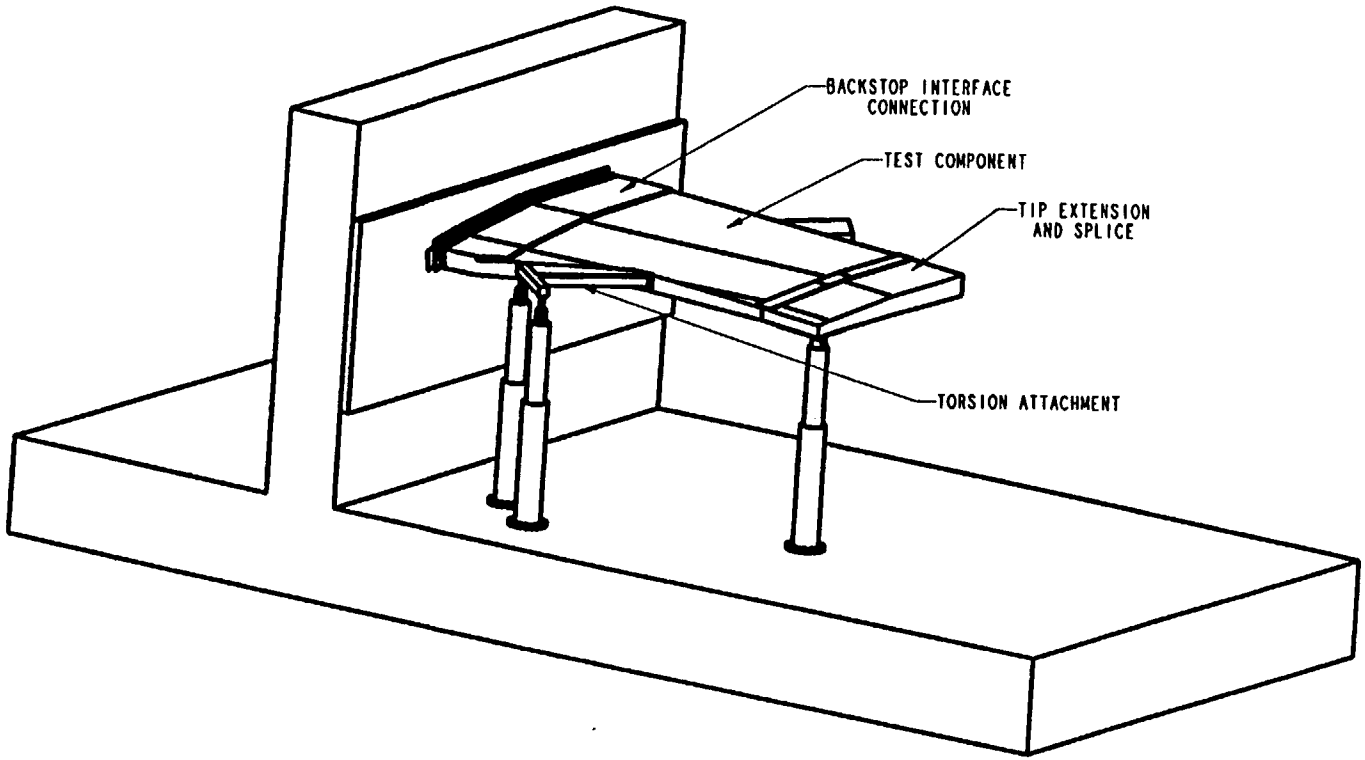

Figure 42.- Actuator layout

Figure 43.- Actuator layout, plan view

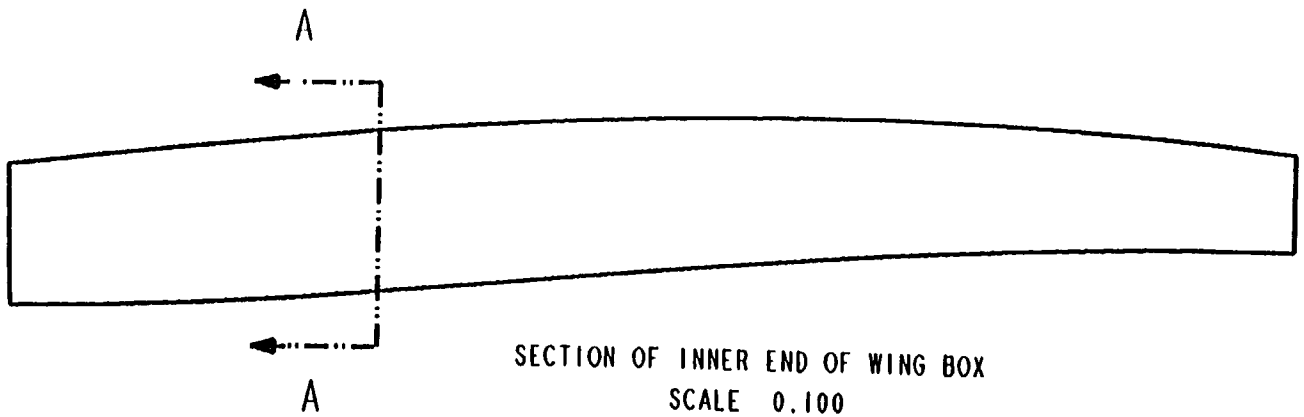

Figure 44.- Wingbox section profiles

REPORT DOCUMENTATION PAGE

Form Approved
OMB No. 0704-0188

1. AGENCY USE ONLY (*Leave blank*)	2. REPORT DATE	3. REPORT TYPE AND DATES COVERED
	July 1996	Contractor Report

4. TITLE AND SUBTITLE

A Study of Facilities and Fixtures for Testing of a High Speed Civil Transport Wing Component

5. FUNDING NUMBERS

C NAS1-19000
WU 537-06-34

6. AUTHOR(S)

J. A. Cerro, R. F. Vause, L. M. Bowman, J. K. Jensen, C. J. Martin, Jr., A. E. Stockwell and W. A. Waters, Jr.

7. PERFORMING ORGANIZATION NAME(S) AND ADDRESS(ES)

Lockheed-Martin Engineering and Sciences
144 Research Drive
Hampton, VA 23666

8. PERFORMING ORGANIZATION REPORT NUMBER

9. SPONSORING / MONITORING AGENCY NAME(S) AND ADDRESS(ES)

National Aeronautics and Space Administration
Langley Research Center
Hampton, VA 23682-0001

10. SPONSORING / MONITORING AGENCY REPORT NUMBER

NASA CR-198352

11. SUPPLEMENTARY NOTES

Langley Technical Monitor: Stephen J. Scotti

12a. DISTRIBUTION / AVAILABILITY STATEMENT

Unclassified - Unlimited

Subject Category 39

12b. DISTRIBUTION CODE

13. ABSTRACT (*Maximum 200 words*)

A study was performed to determine the feasibility of testing a large-scale High Speed Civil Transport wing component in the Structures and Materials Testing Laboratory in Building 1148 at NASA Langley Research Center. The report includes a survey of the electrical and hydraulic resources and identifies the backing structure and floor hard points which would be available for reacting the test loads. The backing structure analysis uses a new finite element model of the floor and backstop support system in the Structures Laboratory. Information on the data acquisition system and the thermal power requirements is also presented. The study identified the hardware that would be required to test a typical component, including the number and arrangement of hydraulic actuators required to simulate expected flight loads. Load introduction and reaction structure concepts were analyzed to investigate the effects of experimentally induced boundary conditions.

14. SUBJECT TERMS

High Speed Civil Transport, structural testing, thermal, finite element, test facilities

15. NUMBER OF PAGES

65

16. PRICE CODE

A04

17. SECURITY CLASSIFICATION OF REPORT	18. SECURITY CLASSIFICATION OF THIS PAGE	19. SECURITY CLASSIFICATION OF ABSTRACT	20. LIMITATION OF ABSTRACT
Unclassified	Unclassified	Unclassified	

NSN 7540-01-280-5500

Standard Form 298 (Rev. 2-89)
Prescribed by ANSI Std. Z39-18
298-102